Electrochemical Impedance Spectroscopy as a Method to Predict Delamination of Coated Steel in Cathodic Disbondment Tests

by

Anand Raghunathan

S.B., Materials Science and Engineering (1996)

Massachusetts Institute of Technology

Submitted to the Department of Materials Science and Engineering
in Partial Fulfillment of the Requirements for the Degree of
Master of Science in Materials Science and Engineering

at the

Massachusetts Institute of Technology

June 1997

Signature of Author.....
Department of Materials Science and Engineering
May 9, 1997

Certified by.....
Ronald M. Latanision
Professor of Materials Science and Engineering
Thesis Supervisor

Accepted by.....
Linn W. Hobbs
John F. Elliot Professor of Materials
Chair, Departmental Committee on Graduate Students

Electrochemical Impedance Spectroscopy as a Method to Predict Delamination of Coated Steel in Cathodic Disbondment Tests

by
Anand Raghunathan

Submitted to the Department of Materials Science and Engineering
on May 9, 1997 in Partial Fulfillment of the Requirements for the Degree of
Master of Science in Materials Science and Engineering

Abstract

A study was undertaken using electrochemical impedance spectroscopy to measure delamination and compare that measurement, which can be performed on the sample repeatedly, with the accepted method of cathodic disbondment (CD) testing, the major drawback of which is that this measurement can only be done once on the sample; in reaching this goal, EIS could be used to predict delamination based on electrochemical values and the relative effects of temperature and pH under these same conditions could also be predicted. Poor prediction capabilities and the variety of testing parameters are the problems with the present cathodic disbondment test method; no analytical correlation of these factors has been reported. These factors will be addressed in this document. Epoxy coated samples were run at a temperature of 65 ^{0}C at -3V vs. SCE polarization in a 3 wt% sodium chloride solution for a period of 20 days. Based on relatively constant increases in capacitance with delamination, a correlation between capacitance and delamination was established. Capacitance values were then estimated for times greater than 4 days; using these capacitance values, predicted delamination values were obtained and compared to observed delaminations. These values are comparable between Day 6 and Day 14. At Day 18 and Day 20, delamination predictions differ from measured values by approximately 35%; however this error decreases when the variation in observed delamination is considered. Therefore, it can be concluded EIS can be used as an effective prediction tool for delamination. Temperature and pH effects on delamination were also studied to determine if predictions could be made through scaling factors for various temperatures and pHs. Although the temperature observations show a good fit to an Arhennius behavior, the calculated activation energy of 330 Joules/mole is far lower then expected for a chemical reaction. This most probably indicates that a more complex delamination mechanism than the one considered in this study exists. A 2.5 fold decrease in delamination was observed in samples tested at an electrolyte pH of 1 when compared to the ambient electrolyte pH of 8. Because the electrochemistry drives an increase in the local pH, predictions in delamination can not be made. However, this study has shown that delamination is reproducible at pH 1 and 8

Thesis Supervisor: Dr. Ronald M. Latanision
Title: Professor of Materials Science and Engineering

Table of Contents

List of Figures

List of Tables

Acknowledgments

Gratitude is extended to the 3M company, the 3M Austin Sector Laboratory, and the Electrical Specialties Division of 3M for allowing me to perform the necessary research for this thesis. A special thanks is extended to Dr. Alan Hulme-Lowe for hiring me into the Austin Sector Lab to perform my graduate research in an industrial setting.

I wish to extend much thanks to Drs. Maureen Fahey and Gary Shreve for their guidance through this project as well with the other projects I was involved in during my seven months at 3M. Thanks is also extended to them for their assistance in data analysis, writing, and editing of this thesis. A special thanks is extended to Susan Wieland for her patience and help with sample preparation. I would also like to thank the scientists and engineers of the 3M Austin Sector Lab for their help during my internship.

Thanks is extended to Professor Ronald Latanision for agreeing to be my thesis supervisor and for his help during the writing of this thesis.

A special thanks should go to my parents and my brother for their lifelong support and encouragement in all tasks I have taken up. Without their support, the research and writing of this thesis would not have been possible.

1 Introduction

1.1 Protection of Steel Pipes

Pipes are used to transport liquid and gaseous materials from extraction points to central processing facilities to consumers. Cost and durability are primary concerns; for these reasons, the majority of these pipes are made of steel because of its strength and toughness [1]. Although there are numerous advantages to using steel, there are a few disadvantages too. The one of most importance involves the ongoing chemical reaction between the iron in steel and oxygen and water in the environment; this phenomenon is better known as corrosion.

Steel pipes, which contain approximately 99% iron, are found in all climate types; under these environmental conditions, iron is thermodynamically driven to corrode. Through this process, a porous brittle iron-oxide layer forms on surface of the steel pipe reducing its mechanical properties. Ultimately this leads to failure which can cause grave ecological disasters creating enormous costs for clean up and replacement of these pipes.

To protect against this, scientists have improved the corrosion resistance of steel through alloying, through cathodic protection, and/or through the use of coatings. Alloying with elements such as nickel, manganese, silicon, and chromium produces specialty metals, such as stainless steel. These specialty steels intrinsically resist corrosion because the additives form an impermeable and stable oxide layer on the surface of the steel. As a result, the reactants necessary for the corrosion are able to combine with the iron after very long times. However, the corrosion resistance of stainless steel usually

comes at a much higher cost and could effect performance when compared to that of ordinary steel [2].

Cathodic polarization at -1.5V vs. NHE (normal hydrogen electrode) electrochemically limits corrosion by placing the steel at a prescribed potential through an external source. The potential of the pipe is decreased below the equilibrium corrosion potential thus mitigating this process [1,3]. Figure 1 displays the Pourbaix diagram for iron which shows the thermodynamic stability of iron when placed in aqueous environments under equilibrium conditions [4,5]. The shaded portion of the Pourbaix diagram reveals the pH and potential regimes where corrosion is thermodynamically favored. By increasing (making more positive) the potential of the iron, a stable insoluble oxide forms rendering the surface passive to corrosion. By decreasing the potential (making more negative), the steel enters a regime where it is immune to corrosion. This is the regime of cathodic protection [4,5].

Under cathodic polarization, the metal is thermodynamically stable; oxidation takes place at the anode and not at the steel. However, protection of vast amounts of steel pipes solely through cathodic polarization would require large amounts of current. The high costs associated with this protection method do not make it feasible.

Organic coatings have also been used to protect against corrosion because they provide a barrier to water and oxygen permeation and/or the resistive pathways the corrosion process must follow. Their low cost and good mechanical properties also make them very

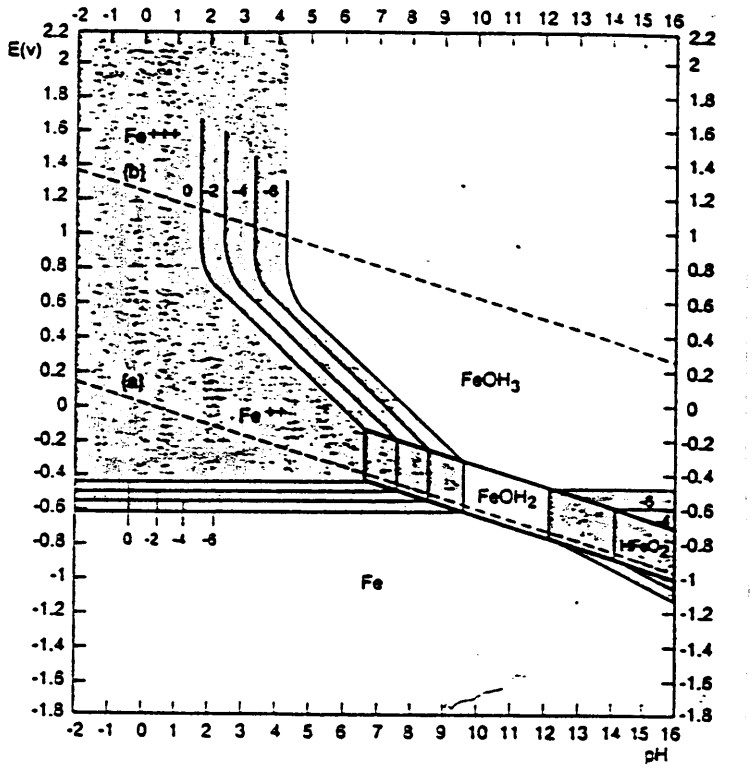

Figure 1. Pourbaix diagram for iron in aqueous media at room temperature. Line *a* represents hydrogen evolution, Line *b* represents oxygen reduction. Equilibrium species are listed. The shaded regions indicate active corrosion [4].

attractive. These organic coatings adhere well to the steel, have long service lives, and endure the abuse expected during their transport and handling (Figure 2). However, upon the development of defect sites such as nicks and scratches, corrosion takes place as with uncoated steel. The corrosion process can then proceed under the coating, delaminating more area, and weakening more and more steel.

By combining the previous two methods of protection, a better and more economical alternative for protecting steel pipes has been developed. This alternative method involves the use of low dielectric coatings with cathodic polarization. The low dielectric coating behaves as both a barrier to the water and oxygen molecules and as an insulator which limits the overall potential required for cathodic polarization. Cathodic polarization protects the steel against corrosion at defect sites. When organic coatings fail at nicks and scratches, cathodic polarization artificially places the exposed steel at a potential lower than the corrosion potential thereby suppressing this reaction.

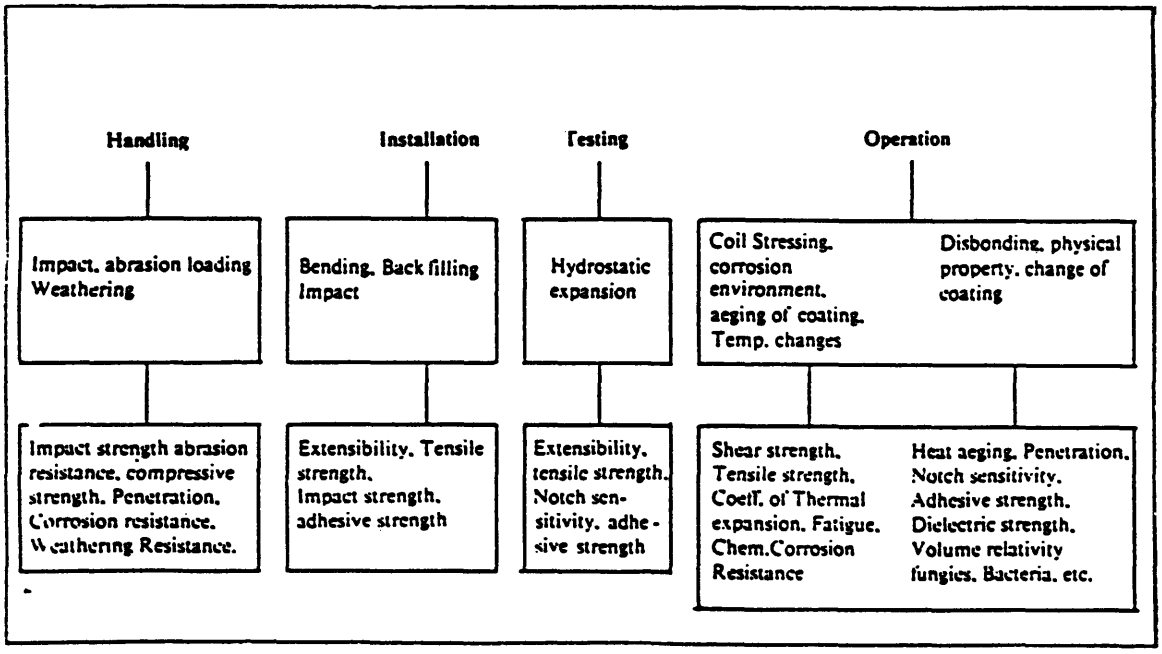

Figure 2. Coating handling before installation and during service indicating what properties are required to be used on steel pipes [1].

1.2 Corrosion

1.2.1 Corrosion Electrochemistry

In order to effectively protect steel pipes, the complex process of corrosion must be understood. Corrosion is an electrochemical process between the surface of a metal and the materials with which it is in contact [4]. In the specific case of steel, iron reacts with water and oxygen [1]. In an acidic environments, soluble iron ions, hydrogen gas, and water are produced (Equations 1-3). In more basic environments, the reactions in equations 4-5 take place yielding insoluble oxide products [1,2,6].

$$Fe \longrightarrow Fe^{2+} + 2e^- \quad (1)$$

$$H^+ + e^- \longrightarrow \tfrac{1}{2} H_2 \quad (2)$$

$$2H^+ + \tfrac{1}{2}O_2 + 2e^- \longrightarrow H_2O \quad (3)$$

$$Fe^{2+} + H_2O + \tfrac{1}{2}O_2 \longrightarrow Fe(OH)_2 \quad (4)$$

$$Fe(OH)_2 + \tfrac{1}{2}H_2O + \tfrac{1}{4}O_2 \longrightarrow Fe(OH)_3 \quad (5)$$

The species produced through the reactions in equations 4 and 5 passivate the steel surface by forming a barrier layer through which the oxygen and water must diffuse through to continue the corrosion process.

However, the corrosion process is further complicated when chloride ions are introduced into the aqueous media under equilibrium conditions. These chloride ions

break down or prevent the formation of the passive oxide layer seen in equations 4-5. This results in an increase in the corrosion process [2].

Cathodic polarization of the steel electrochemically limits corrosion by forcing all the reactions to take place at the anode, or the metal electrode. Electrons are supplied to the steel from impressed currents such that the oxidation reaction of the iron seen in equation 1 is suppressed at the steel surface [1]. Cathodic polarization also limits the effects the chlorine ions has in the aqueous media [2].

1.2.2 Factors Affecting Corrosion

Like the majority of other chemical reactions, the corrosion process has a number of factors which can aid or hinder it. Three important factors which effect the rate of corrosion are temperature, pH and potential. An increase in temperature causes the corrosion reaction to proceed at an faster rate producing more of the product; as reported by M.H. Nehete, the rate of corrosion attack doubles with every 4.4 ^{0}C increase in temperature [1].

Potential and pH also affect the corrosion process. Their effects have been described for many metals by Pourbaix. As described earlier, the potential at which the steel is under can produce a passivation layer to protect against corrosion or allow the steel to be immune to corrosion depending on what type of polarization is applied.

Altering the pH of the system can also place the iron in a passive, corrosive, or immune state. Figure 1 shows the Pourbaix diagram for iron under equilibrium conditions

in aqueous media;, iron is stable in aqueous environments at low pHs with cathodic potentials less than -0.6V vs. NHE.

From the Pourbaix diagram in Figure 1, it appears that by placing steel at potentials much lower then -3V vs. NHE throughout the pH range, corrosion can be halted. In reality, most steel pipes are kept at or near -1.5V vs. NHE cathodic polarization for two reasons. The primary reason is that cathodic polarization produces hydrogen from the reduction of water. Large cathodic potentials can produce enough hydrogen to diffuse into the steel. As a result, hydrogen embrittlement of the steel can become a significant failure problem. The second reason for not placing these pipes at such low potentials is the costs required to maintain such potentials.

1.3 Failure of Protective Coatings

To limit the costs associated with cathodic polarization, protective coatings are applied to pipes. During service, the pipe is usually undisturbed, however there are numerous opportunities for partial or total coating failure on the steel pipes either before installation or during the service life. The primary cause of failure in polymeric coatings is loss of adhesion to the substrate and damage to the coatings [1]. Delamination can take place either in intact areas or at defects sites. In intact areas, delamination is caused by the permeation of water and other species into the interface between the coating and the steel. There, water along with the ions initiates underfilm corrosion thereby weakening the bonds between the coating and the steel thus exposing more reaction area. This leads to

greater amounts of delamination, as well as the initiation of blistering in the coating, and can produce a water phase at the coating/metal interface [7].

In damaged regions, polarization applied to the steel initiates a current flow through the defect site which can accelerate the delamination of the polymer coating; this phenomenon is known as cathodic disbondment. Cathodic disbondment is caused by two main mechanisms. As the current flows through the defect, water and oxygen are reduced producing hydroxide groups and hydrogen gas. The increased alkalinity in this region can loosen the coating through the dissolution of oxides on the metal, through attack of the polymer film, or through attack of the metal/polymer interface [7]. In addition, as seen in the Pourbaix diagram in Figure 1, the increased alkalinity can also move the steel from a region of stability to a more corrosive region under equilibrium conditions. Second, the hydrogen gas escapes in the form of bubbles. These bubbles form at exposed areas of the steel including at scratches and nicks as well as under areas of coating delamination. As the bubbles tries to escape from under the coating, it exhibits a lifting-type force [2]. This force can expose new regions of steel increasing this cathodic disbondment effect.

1.4 Evaluation of Protective Coatings for Steel Pipes

1.4.1 Traditional Methods

Because of the cathodic disbondment effect, coatings are evaluated for their disbondment properties before being used in the field. An accelerated test to evaluate adhesion of a coating to the steel under service conditions is described in the ASTM G8 -

Standard Test Methods for Cathodic Disbonding of Pipeline Coatings [8]. In this test, a mechanically cleaned and roughened steel plate is coated with a polymer. A holiday, an intentional defect, is drilled into the coating, and the sample is assembled into a test cell (Figure 3).

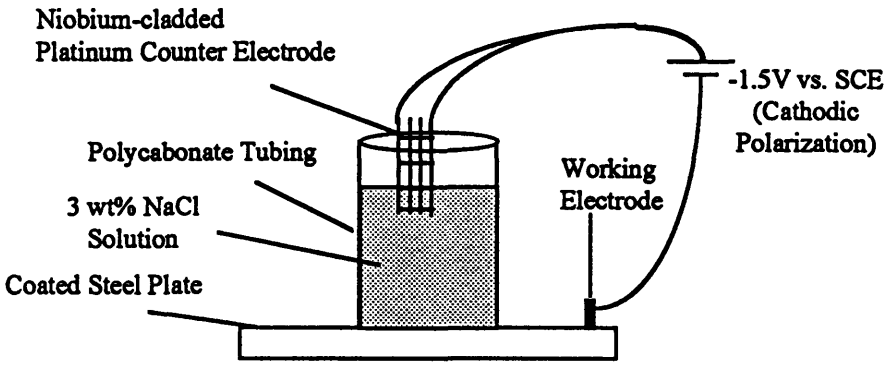

Figure 3. Sample electrochemical test cell used in the evaluation of coatings in accordance with the ASTM Standard G8 [3].

The test sample is exposed to a harsh electrolyte, such as 3 wt% sodium chloride in water, polarized to the potential, -1.5V vs. SCE (saturated calomel electrode), seen during service, and run for a predetermined amount of time. The offset between NHE and SCE is approximately 0.24V [9]. The temperature of the sample may be elevated to further accelerate the effects. This test generates hydrogen gas and hydroxide groups from the reduction of water at the defect site; the gas escapes as bubbles while the hydroxide groups remain in solution generally increasing the local pH. Although the ASTM standards prescribes a testing potential of -1.5V vs. SCE, many test methods used

in industry use much more severe potentials such as -3V vs. SCE to observe the maximum effects of cathodic disbondment.

At the end of the testing, the sample is removed, and a blade is used to cut a star pattern onto the surface of the coating (Figure 4a). A blunt knife is then used to mechanically delaminate the disbonded coating; the amount of exposed steel is related to the coating's ability to resist delamination under cathodic protection (Figure 4b). Coatings that meet or exceed specifications, such as those from British Gas Business Engineering Technical Specification and National Standards of Canada have demonstrated service lives in excess of 35 years [10,11,12]. These standards specify of no more than 5 mmr (millimeter radius) debondment after 30 days at -1.5V vs SCE in 3 wt% NaCl at 23 ^{0}C. This test is a primary screening tool for coatings because of the correlation between field data and the test data.

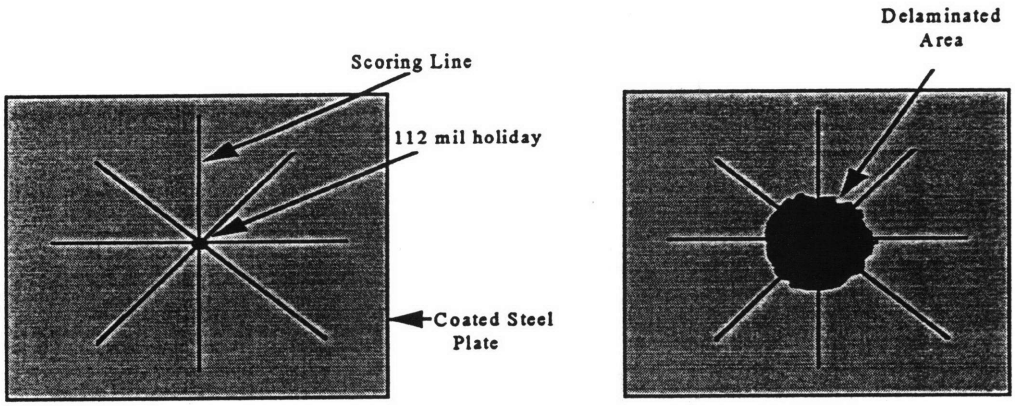

Figure 4 a) Scoring of coating after cathodic disbondment test, b) Delaminated area of coating after cathodic disbondment test.

1.4.2 Developmental Test Methods-Electrochemical Impedance Spectroscopy

1.4.2.1 Background

Two problems exist with the present method for coating evaluation. The first is its inability to predict delamination at longer times than the test is run. A number of experimental test methods have been investigated for prediction of delamination; few have been successfully correlated with coating lifetime under actual conditions [13].

The second problem involves the variety of testing parameters used in coating evaluation. Although ASTM has prescribed a certain range of parameters by which the testing should be performed, companies in the pipeline and coating industries often set their own conditions and specifications. Some may decide to test with different holiday sizes, or different concentration of solute in solution, or any other combination of changes. The different test parameters throughout industry cause some difficulty in comparisons of the effectiveness of coatings. To date, no analytical correlation of these factors has been reported. This thesis will address this problem.

1.4.2.2 Impedance Test Method

These problems have spurred a good deal of research on alternative test methods for coating evaluations. One promising test method is electrochemical impedance spectroscopy (EIS) [14,15,16]. EIS involves the application of a sinusoidal voltage to an electrode over a frequency range; a resulting current from the applied voltage is then

measured (Figure 5) [13]. Impedance is calculated as the ratio of the applied voltage to the current response of the system as a function of frequency where $\omega=2\pi f$ (angular frequency) (Equation 6).

$$Z(\omega)=\frac{V(\omega)}{I(\omega)} \tag{6}$$

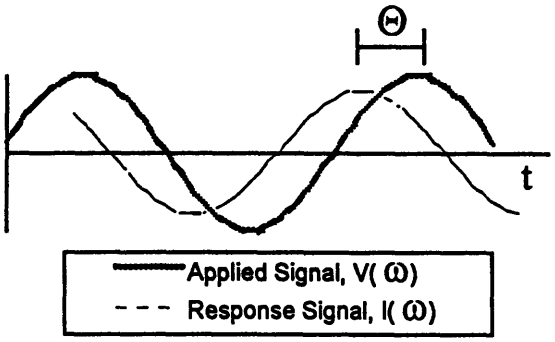

Figure 5. Applied and response signal of impedance spectroscopy. Current I(ω) lags voltage V(ω) by phase angle Θ [17]

Theta (Θ) is the phase angle of the system which reveals by how much the response current is out of phase with the applied voltage and is related to the capacitive components of the system. In addition, the phase angle is frequency dependent; changes in |Z| (impedance) and Θ with frequency provide information on the system under study allowing for modeling of the system.

An example of an impedance scan is shown in Figure 6. The scans are represented in three different type sketches. Figures 6a & b are Bode plots of a hypothetical system -

Figure 6a sketches the logarithmic magnitude of impedance as a function of the logarithmic frequency while Figure 6b represents the phase angle (Θ) as a function of logarithmic frequency. When analyzed together, these two plots define the impedance vector of the system. Impedance can also be presented in terms of real and imaginary impedance components as seen from the Nyquist plot (Figure 6c).

In order to fully understand the system response, these impedance plots are fit to equivalent circuits through numerical analysis [13]. Over the scanned frequency range, a close match in the response of an equivalent circuit with that of the electrochemical cell insures that the impedance data can be broken into discrete components. These components can be any combination of resistors, capacitors, inductors, and other complicated elements formed into a circuit though components should be physically realistic [13]. Upon identification of an acceptable circuit, a total impedance equation can be derived for the system through the addition of impedance values for each individual element. Table 1 shows the simplest elements and their impedance calculations.

Each individual element possesses its own characteristic impedance; resistive elements are frequency independent, while capacitive and inductive elements have large dependencies on low and high frequencies respectively [7]. In corrosion systems, inductors are not generally valid because apparent inductance infers that the system in not in a steady state on the time scale of the measurement. This would therefore invalidate EIS analysis.

With the equivalent circuit and total impedance equation determined, the analysis of the impedance data continues by assigning each element to a particular part of the electrochemical system. It is this last step in the analysis that makes EIS a valid

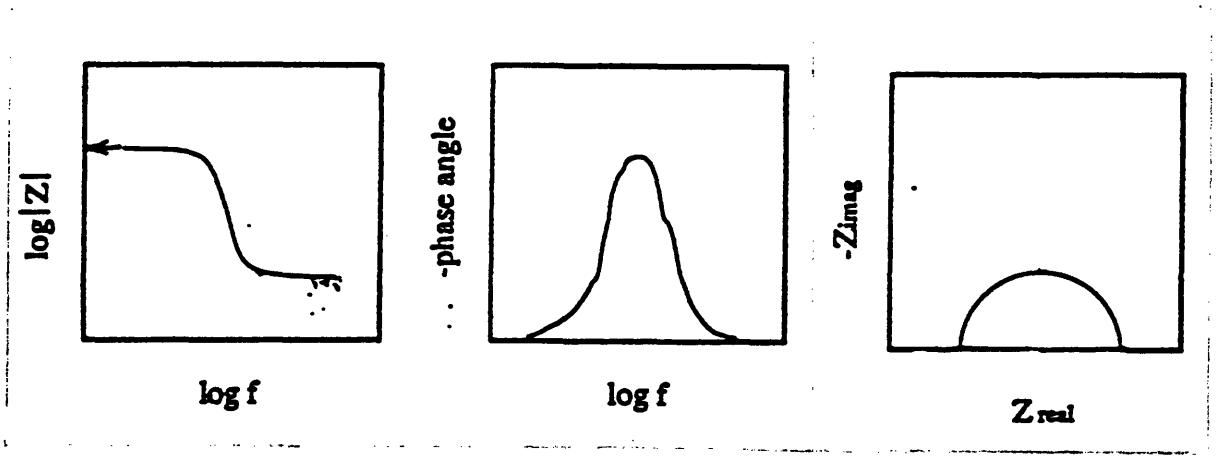

Figure 6. a) Bode impedance plot, b) Bode phase angle plot, c) Nyquist plot for a system described by $Z = Z' + iZ'' = |Z| (\cos\Theta + i \sin\Theta) = Z_{real} - iZ_{imaginary}$ [7].

Table 1 Impedance calculations for the most often used circuit elements.

Element Type	Impedance Calculation
Resistor	$Z_R = R$
Capacitor	$Z_C = \frac{1}{-i\omega C}$
Inductor	$Z_L = -i\omega L$

technique in the evaluation of samples. Changes in the particular elements of the equivalent circuit may be attributed to changes in the cell. Figure 7 represents a coating

with a defect in it. A sample equivalent circuit which describes the system is overlaid on the sample; each element of the circuit is paired with a particular part of the cell.

$R_{solution}$ is the solution resistance or the effective potential drop between the working and the reference electrode. Coating capacitance is given by $C_{coating}$, , and R_{pore} is the resistance or the potential drop from the open end of the defect to the metal surface due to the electrolyte penetration. The R_{ct} is the charge transfer resistance which represents the charge leakage at the interface of the solution and metal. $Z_{transport}$ is the impedance associated with the transport of material from the metal to the solution [18]. Finally, $C_{double\ layer}$ is the double layer capacitance which arises when metals are placed in an electrolyte. The ions in solution spontaneously arrange themselves at the metal-solution interface. The electrical behavior of the double layer can be modeled by a dual plate capacitor [4].

EIS is used to evaluate a number of systems including coatings, batteries, and numerous corrosion systems [18,19]. This study will focus on the use of EIS for study of coatings and corrosion systems simultaneously.

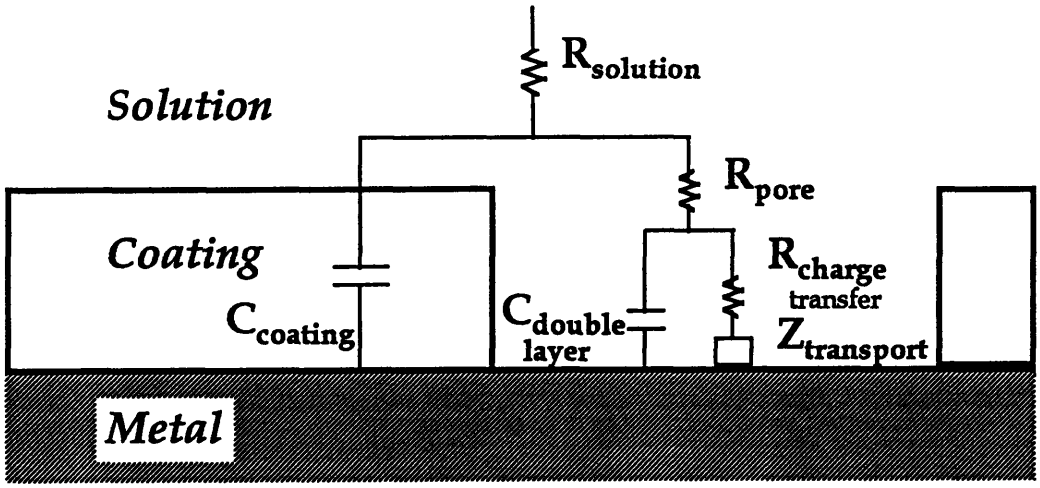

Figure 7. Possible electrochemical cell with equivalent circuit overlay. Each component of the circuit is assigned to a particular part of the electrochemical cell [17].

1.5 Research Objectives and Significance

In the present method for coating evaluation, there is much difficulty in predicting delamination at various testing times. Quantitative values for delamination can be obtained solely through actual testing of samples which is a long and time-consuming process which is expensive.

The goal of this study is to determine if EIS can be used as a predicting tool for coating delamination. As seen from Equation 8,

$$C = \frac{\kappa \varepsilon_0 A}{d} \tag{7}$$

capacitance is linearly proportional to area [20]. Therefore, if capacitance (measured through electrochemical methods) and delamination area (observed through physical delamination of the specimen) can be correlated with each other, the delamination for testing times could be predicted through a non-intrusive method by measurement of sample's capacitance; using predicted values, estimated delamination values over a range of temperatures and pHs could also be obtained.

Capacitance trends were obtained from the fitting of impedance scans to a ZARC-Cole distributed element equivalent circuit. Cathodic disbondment tests, done in accordance with modified ASTM G8, have shown that disbonded regions of the epoxy

coatings peel easily from the steel and delamination extends radially outward from the defect site. This was monitored physically by mechanical delamination of the coating.

The significance of this approach is that a new *in situ* test method has been developed to evaluate coatings for their adhesion properties when coated onto metal and polarized as in the cathodic disbondment test. Delamination can be predicted for various testing times. The effects of temperature and pH can also be observed. Finally, after further study and refinement, this test method could be the main method by which coatings are evaluated by which would save significant amounts of time and make results easily comparable.

2 Experimental

2.1 Sample Preparation

2.1.1 Production of coated plates

Hot rolled steel with dimensions 4.5" X 4.5"X 0.5" was obtained and placed into containers of methyl-ethyl ketone for three days to strip the surface of any oils. The steel plates were then pulled from the solvent, dried with compressed air, and grit blasted with a grit size of 25GL until the surface showed a white metal finish. These samples were then placed into a convection oven. They were allowed to heat overnight at a temperature of 240 ^{0}C.

The coating used in this experiment was the Scotchcast brand 206N Fast Epoxy © manufactured by the 3M Company. This powered epoxy was divided into metal cans and dried in a vacuum at -30 in-Hg for at least one day before being used.

Coating the steel plates using an electrostatic spray gun produced coating which were too thick for use in this study. Thinner coatings were produced by dip-coating in a fluidized bath. A vibrating plate and an air jet were connected to the fluidized bath to insure that the epoxy never settled which would have caused uneven coatings. Vise Grip pliers were used to remove the heated steel plates from the oven; the plates were manually dipped into the bubbling epoxy solution for 1.5 seconds. After the dipping, the steel samples were placed into a post-curing oven at 232 ^{0}C for three minutes. Following the

post cure, the samples were quenched in water and dried. The coating thickness of each sample was measured; thickness of the samples were 13.8 mils (+/- .68 mils).

2.1.2 Electrochemical Test Cell

To accommodate the steel specimens, specialized fixtures were used. Figure 8 shows an example of the test cell.

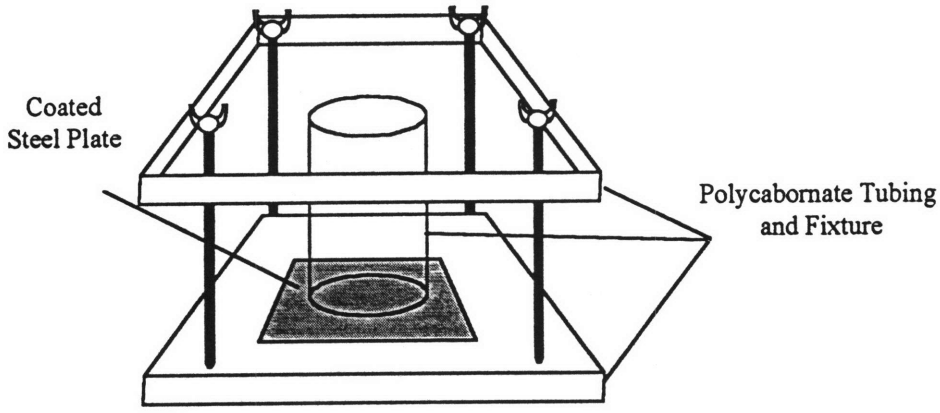

Figure 8. Electrochemical test cell used in the impedance testing [17].

The test area of these plates was isolated by using a silicone rubber gasket between the polycarbonate tubing and the bottom plate. Screws were used to tighten the tubing and silicone seal to the bottom plate making it water tight. The electrolyte used in this study was 3 wt% sodium chloride (Aldrich Chemicals) in deionized water.

To accelerate the test conditions, VWR Model 210 Mini Hot Plates were placed under the electrochemical cells. When the hot plates were used, $\frac{1}{8}$" thick aluminum plates were used in lieu of the bottom polycarbonate plate to avoid melting and adhesion between the hot plate and the polycarbonate.

Before drilling the defect, individual samples were tested by impedance spectroscopy to insure that the coatings were intact. After this initial test, the steel samples were transported to a drill press where 2 holes were drilled, a .5" deep hole at the edge for the working electrode screw and a shallow 112 mil hole in the center for the holiday.

A 112 mil holiday was used for all experiments because it allowed the test equipment to sustain adequate potential on the samples and did not allow hydrogen bubble entrapment in the defect. The defect was drilled through the coating to the steel with a flattened drill bit so that the surface in the defect could be approximated as planar, simplifying area calculations. The plate was placed in the test fixture which was then filled with electrolyte.

2.2 Testing Equipment

2.2.1 Electrode types

A three electrode method, working, counter, and reference electrode, was used to obtain the impedance scans. Electrical contact to the working electrode was provided by a metal screw in the steel plate. The counter electrode was a mesh of niobium clad with

platinum (Plating Supplies International, Inc.). The reference electrode used for testing was the Accumet Saturated Calomel Electrode (Fisher Scientific Accumet catalog number 13-620-51) .

2.2.2 Impedance Test Equipment

Impedance measurements were taken using various instruments connected through a personal computer. A model 283 potentiostat made by EG&G (Princeton Applied Research) and the SI 1255 Schlumberger Frequency Analyzer were connected to each other as the primary impedance station. Two EG&G model 314 multiplexers were added to the impedance testing station. The multiplexers were connected to the potentiostat and the PC allowing for the testing of up to 16 different cells through individual potentiostat cards. The cards also allowed specimens to be kept under potential control between impedance scans for the duration of testing. Figure 9 shows a schematic sketch of the test equipment setup for one of the 16 cells hooked up to the multiplexer.

2.3 Impedance Measurements and Analysis

Each electrochemical cell was kept under a -3V vs. SCE polarization by the multiplexer system. The ZPLOT software written by the Scribner Associates, Inc was used to control the frequency response analyzer, potentiostat, and the multiplexer. ZPLOT was also used to perform the impedance scans. Standards parameters for the scans were 10^6 to 10^0 Hz, -1.5 V DC vs. SCE and 100 mV AC. Impedance data was

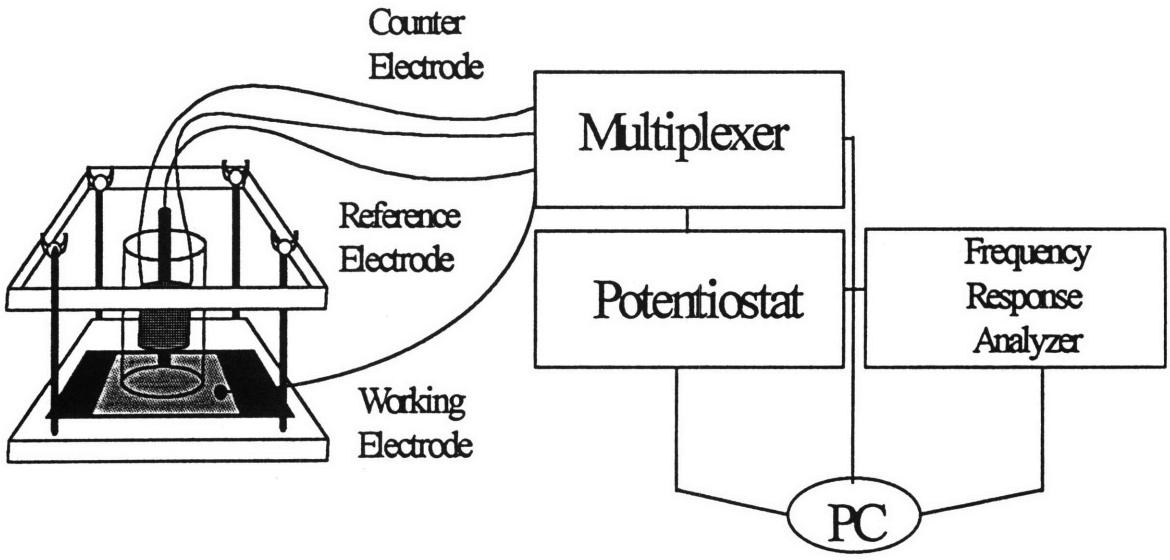

Figure 9. Impedance testing setup [17]

reviewed and fit with equivalent circuit models using the program ZVIEW for Windows also written by the Scribner Associates, Inc. Data was analyzed using Microsoft Excel and the regression was done using the linear fitting function in this same program. Trendlines in the capacitance vs. delamination plots were fit to an intercept of 0 so that the initial capacitance associated with the defect can be accounted for.

The setup and the characterization of the EG&G model 314 multiplexer was performed before this study was begun; its impedance capabilities and limitations were determined. It was observed that the 314 multiplexers had an impedance sensitivity up to 10^8 Ohms at a frequency range of 10^{-1} HZ. From these characterization tests, it was also determined that the sensitivity regime of the expanded EIS setup was between 10^5 to 10^0 Hz.

After these tests, impedance scans were run on the coated steel substrates. Intact samples possess capacitance values from these sample were around $5*10^{-11}$ Farads. Scans were then run on sample with the 112 mil macroscopic defect. The scans on the samples with defects showed two transients; Figure 10 shows the typical Bode impedance and Nyquist plots of the epoxy-coated steel samples. As seen in the Bode plots, two time transients (brief oscillations in the impedance data) appear -one in the 10^6-10^5 high frequency range, and another in the range of 10^3 - 10^1 Hz. These transients are better observed in the Nyquist plot. Two semi-circles appears in the impedance scan; the larger semi-circle is associated with the medium frequency transient. It is in this regime that is of interest in these corrosion studies. The smaller semi-circle arises from the first transient at the high frequency regime.

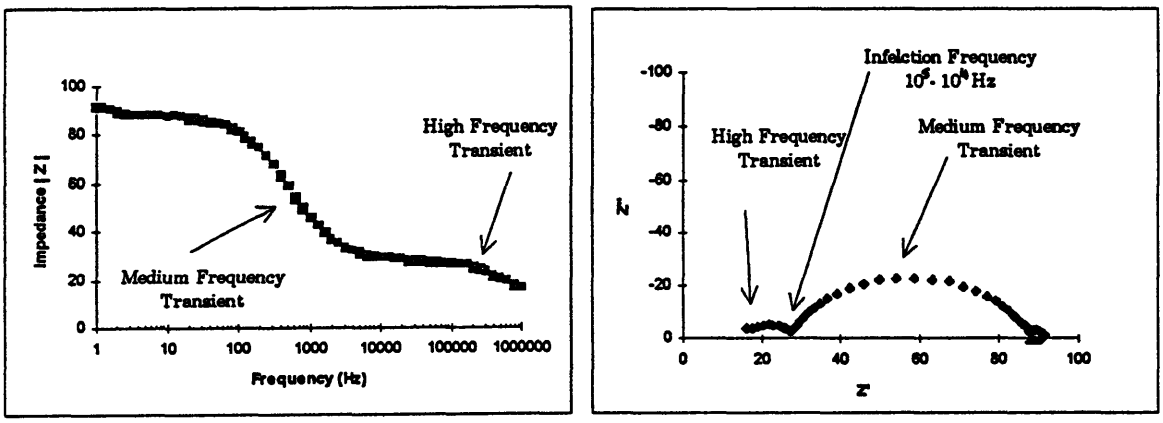

Figure 10. Sample impedance plots from the epoxy coated steel samples kept at -3V polarization for the duration of the test. Impedance scans were run at 100 mV at -1.5 V DC vs. SCE from 10^6 to 10^0 Hz. a) Bode impedance plot over the scanned range. b) Nyquist plot over that same frequency range. The inflection frequency occurs between 10^5 and 10^4 Hz.

Because this transient displayed a dependence on frequency, it was associated with an external capacitance. In order to quantify this mysterious capacitance, a systematic study was performed.

This extra capacitance was initially hypothesized to be associated with the poorly shielded cables between the multiplexer and the potentiostat, but impedance scans run on aircells, 1000 Ω resistors, and scans on other sample types confirmed this was not the case. The reference electrode was then studied by comparing impedance scans from a saturated calomel electrode with that of a silver/silver chloride electrode.

It was determined that this extra capacitance was associated with the SCE reference electrode. Zhang *et al.* also have reported observing this extra capacitance in the higher frequency range of their impedance systems when using a SCE reference electrode [21]. Through their work, it was determined that the reference electrode capacitance is dependent upon solution resistance, capacitance of the reference electrode, and the potentiostat input capacitance. Based on this conclusion, this extra capacitance has been considered an artifact of the system and has since then been dismissed in the data analysis.

2.4 Testing

Tests were run for 20 days; each samples was run at -3V vs. SCE at 65 ^{0}C in a 3 wt% NaCl electrolyte. Specimens were removed on days 1, 2, 4, 6 and every other succeeding day till day 20. The effects of temperature and pH on delamination were also

studied. Temperature test parameters included running specimens at room temperature (22 ^{0}C) , 65 ^{0}C, and 80 ^{0}C for a period of 6 and 10 days at -3V vs. SCE, and in 3wt% NaCl solution. pH effects were tested by observing delamination results from samples which were run with a 3 wt% NaCl solution adjusted to a pH of 1 and the ambient pH of the 3 wt% NaCl solution which was around 8.

Upon completion of the test, each sample pulled from the testing apparatus was drained of the electrolyte, rinsed with deionized water, and allowed to dry for one hour. A knife was used to cut a star pattern onto the coating from the defect radially outward. The knife tip was then used to mechanically delaminated the sample similar to that seen in Figure 4b. The delaminated epoxy lifted from the steel easily; this was continued until no longer possible. To determine the delaminated area and to facilitate the area calculation, samples were photocopied at 150% magnification. The delaminated section in the copy was cut and weighed. Delamination area was measured by the weight of the photocopy. Figure 11 shows an example of a delaminated sample.

Accepted protocols specify coating delamination in terms of millimeter-radius disbondment (mmr) and not delamination weight. Therefore, a conversion factor between these two was determined; this factor was calculated from the initial holiday radius and its photocopied weight at 150% magnification. This factor was calculated to be .04233 cm^2/mg. The error from this calculation is approximately .02%, which is small enough to be accepted as a reasonable conversion factor. Table 2 shows the delamination weights and their conversion to millimeter-radius disbondment. Care must be taken when

comparing sample delamination radii to other specimens as delamination radii were calculated from delamination weights which were magnified by 150%.

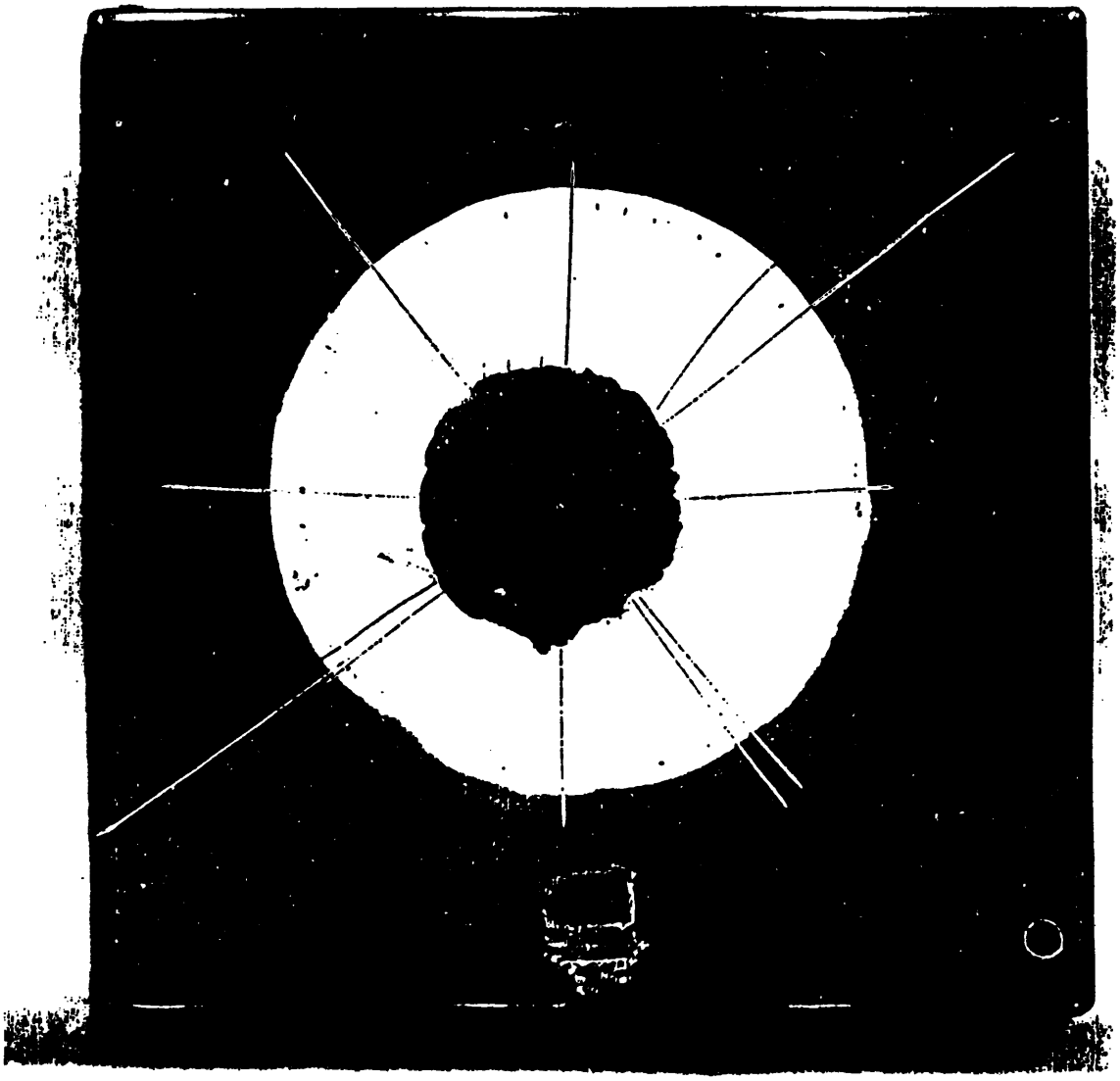

Figure 11. Photocopy of delaminated sample at 150 % magnification. The black core reveal the delaminated areas. It was this section which was cut and weighed to determine amount of delamination.

Table 2. Delamination weights and their conversion to the industry standard - millimeter radius disbondment (mmr) for the non-standard conditions of 65 ^{0}C, at -3V vs. SCE, in a 3wt% NaCl electrolyte..

Test Day	Delamination Weight (mg)	Converted Disbondment (mmr)
0	1.5	1.42
1	9.5	3.57
2	22.5	5.50
4	44.0	7.64

3 Results and Discussion

3.1 Limitations with Impedance Data

Electrochemical impedance spectroscopy (EIS) has been used in the evaluation of coatings to extract information concerning degradation and reactions in confined regions; however since work is still being done to fully understand its capabilities, problems with obtaining and analyzing EIS data are widespread. EIS methods such as Most Probable Impedance Equivalent Circuit (MPI) and Breakpoint Frequency (BF) which were once thought to provide accurate representations of systems are now being challenged [13,22,23].

The following techniques were used to limit the complications and inconsistencies incurred when using EIS. First, to limit the discrepancies associated with analyzing individual impedance scans, trends in the data were analyzed. In this manner, the general tendencies of this system can be better understood and predictions be made.

Second, by observing trends in the capacitance data, the controversial issue of whether the measured capacitance is from the double layer or from an electrified surface (where ions permeate the coating and arrive at the polymer/steel interface and separate based on charge) is avoided. No study was undertaken to link these two together. However, two points in this study indicate that the measured capacitance could be associated the double layer capacitance. First, the magnitude of system's capacitance (10-40 μFarads/cm2) are comparable to double layer capacitance magnitudes observed by

other researchers [24,25]. Second, since capacitance increases consistently with delamination as seen in Figure 12 and 13, it appears that the delamination is causing the increase in capacitance. Therefore from first approximations, this capacitance may be associated with the double layer but must be proven before concrete conclusions may arrived at.

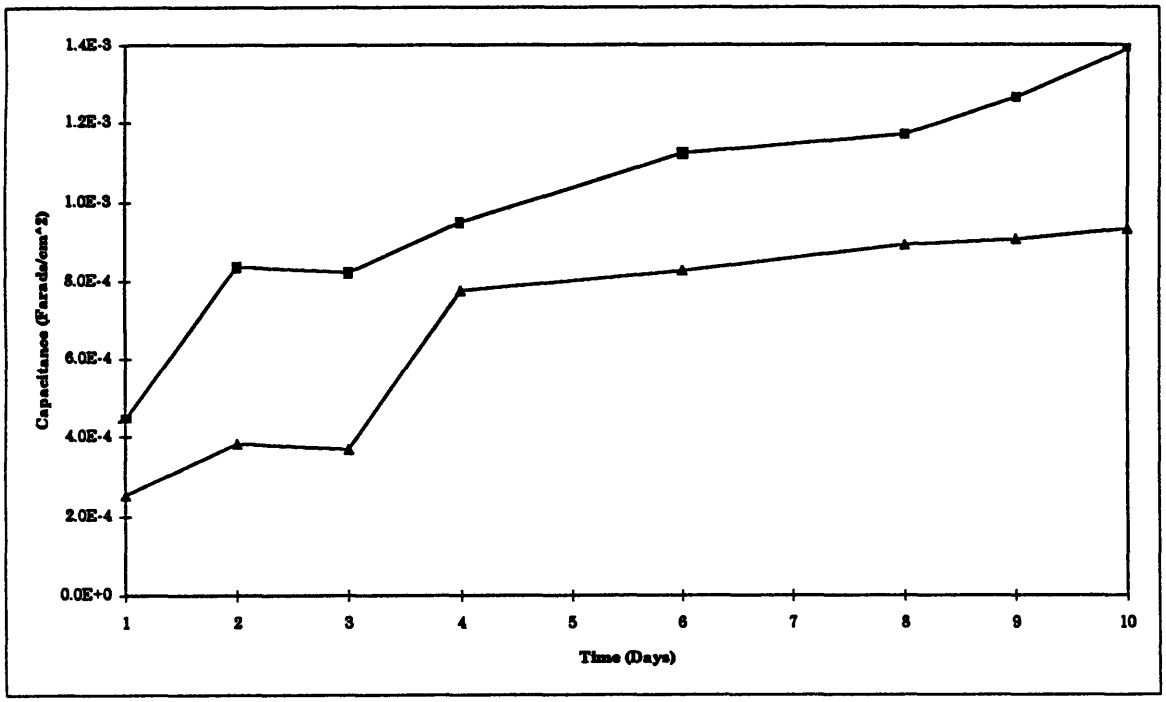

Figure 12. Calculated T_{DE} capacitance from two different samples. Fit capacitance increase with time as more delamination is takes place.

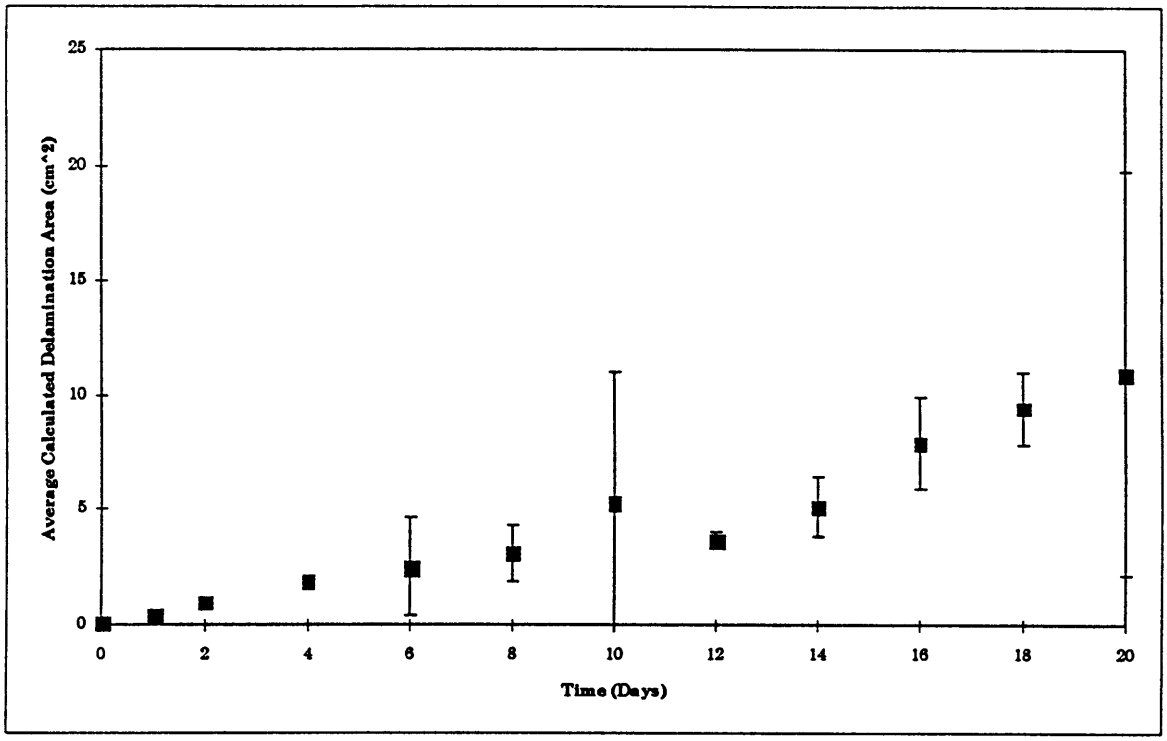

Figure 13 Delamination vs. time trends. Delamination increase with time as does variability between samples.

3.2 Impedance Analysis

3.2.1 Equivalent Circuit Fitting

The impedance response of the system in this study was fit with numerical analysis to a Zarc-Cole equivalent circuit; Figure 14 identifies this circuit which possesses a distributive element [26]. Figure 15 displays how this special element can be represented [26]. R_{DE} and T_{DE} are representative of the resistive and capacitive portions of the distributed element while the >> symbol represents the constant phase element.

The distributed element couples both capacitive and resistive behaviors; the extent of one behavior type over the other is determined by observing the exponent ϕ which

varies between 0 and 1. A ϕ value of 0 indicates resistive behavior while a ϕ value of 1 indicates pure capacitive behavior. The ϕ values of the samples in this test varied between .65 and .9 indicating that the distributed element was dominated by capacitive behavior.

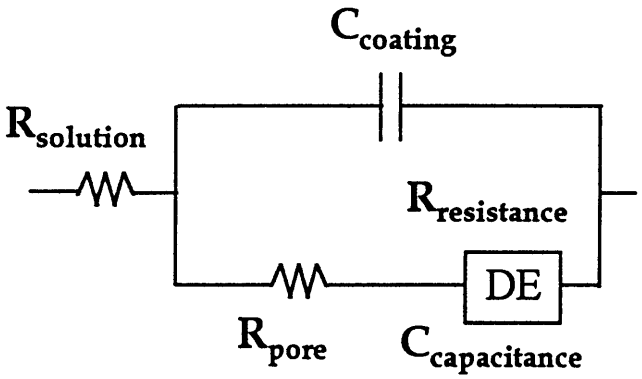

Figure 14 Equivalent circuit which best matches the response of the electrochemical cell. Each component is associated with a physical part of the electrochemical cell. DE is the distributed element used which is associated with the steel surface [26].

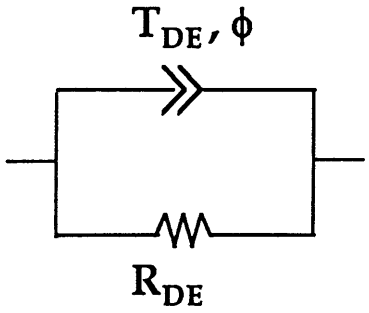

Figure 15 Component makeup of the Zarc-Cole distributive element (DE) from Figure 11 which is represented with a constant phase element (CPE), >> which is best modeled as a capacitive element T_{DE} and a phase angle component ϕ which indicates what type of behavior dominates the system in parallel with a resistive element [26].

Figures 16a, b, & c show the impedance data for a tested sample; the impedance response from the equivalent circuit is overlaid. The fit of the equivalent circuit with the electrochemical cell is good. Error values are quite low; the error range for the fit elements was between 3 and 10% for the duration of the testing for each individual element.

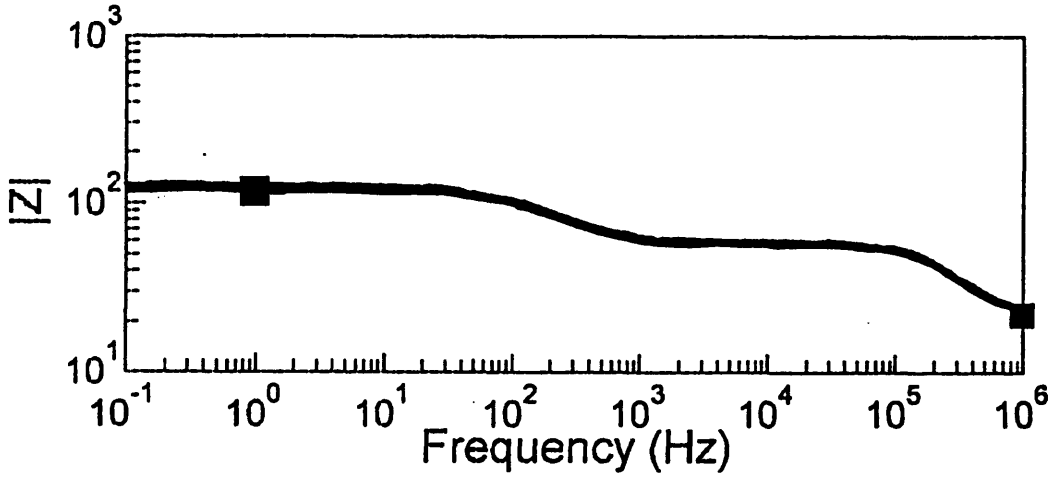

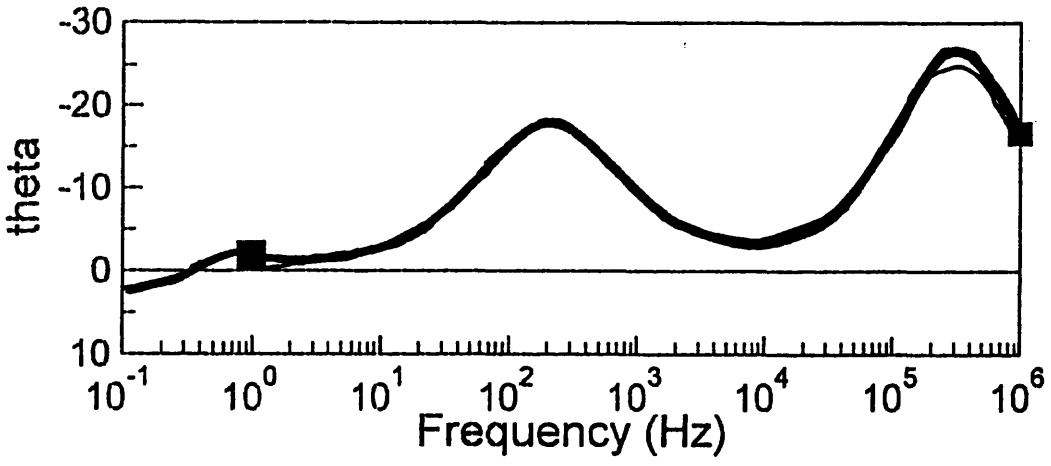

16a) & 16b)

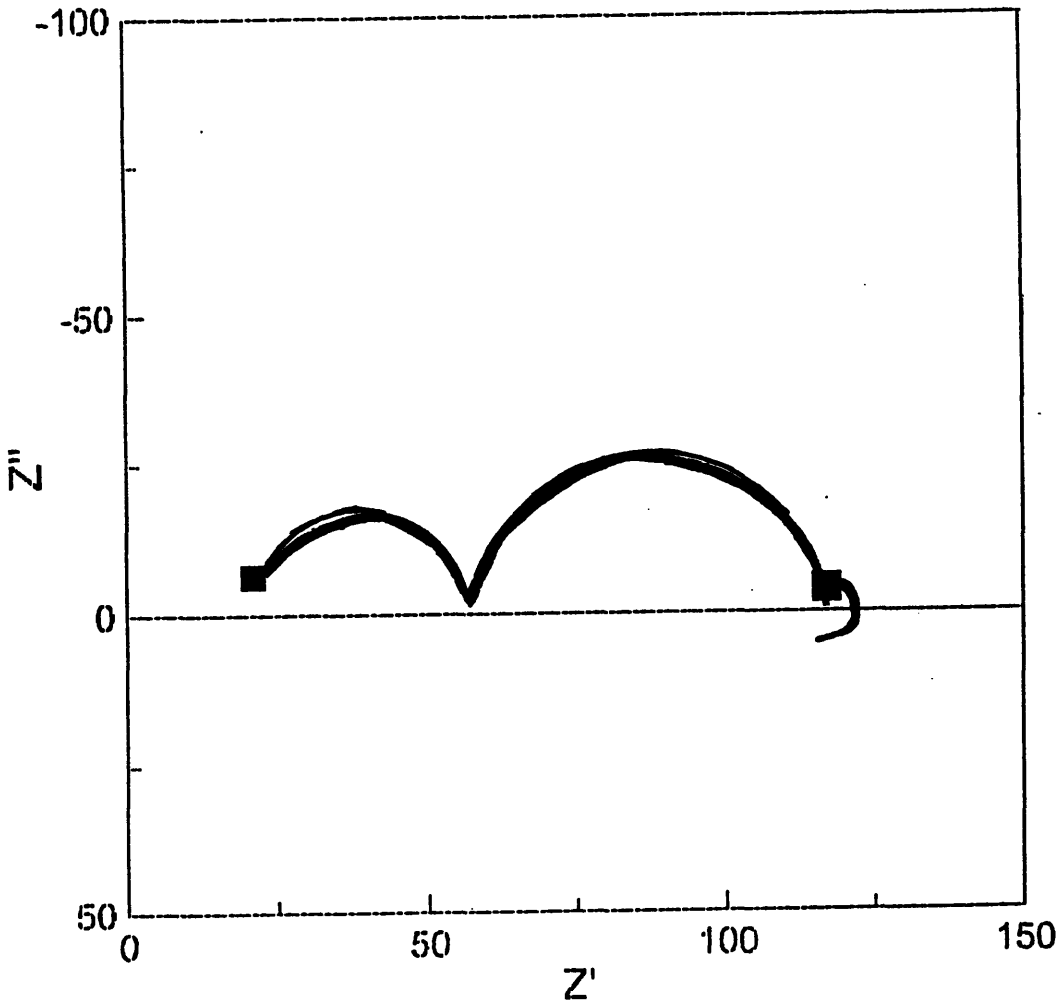

16c)

Figure 16 . Equivalent circuit response overlaid with the response of the electrochemical cell. a) Bode impedance magnitude plots, b) Bode phase angle plots, c) Nyquist real vs. imaginary impedance plot. The dark squares in plot represents the frequency range over which the equivalent circuit fitting was performed. —— represents the impedance scan. ▬▬ represents the equivalent circuit fitting

Upon selection of this equivalent circuit, each component was attributed to a particular aspect of the electrochemical call as seen in Figures 14 and 15. The distributed element was associated with the surface of the steel. The following study was performed to validate this assumption.

Scans were performed on grit-blasted steel in 3 wt% sodium chloride. The impedance scan was fit to the distributed element alone; this produced a good match between the circuit and the electrochemical cell with error ranging between 1 and 10 %. Capacitance values obtained from the bare steel were between 4 and 10 μFarads/cm^2 while the capacitance values obtained from the electrochemical cells with macroscopic defects used in this EIS evaluation study ranged between 10 and 40 μFarads/cm^2.

The observed capacitance can also be calculated from simpler components. By adding capacitance of the metal defect divided by its area percentage to the capacitance of the coating divided by its area percentage the total observed capacitance should be obtained. The calculated capacitance is between 10 and 35 μFarads/cm^2 The similar order of capacitance magnitude measured experimentally and numerically indicates that the exposed surface of the steel in the electrochemical cell can be represented by the distributed element.

Based on the acceptable fit results of the equivalent circuit selected, a total impedance equation was calculated and is shown in Equation 8.

$$Z_T = R_{solution} + \frac{\left[1 + R_{DE} \cdot T_{DE} \cdot (i\omega)^{\phi}\right] + \left[R_{coating} \cdot \left[1 + R_{DE} \cdot T_{DE} \cdot (i\omega)^{\phi}\right] + R_{DE}\right] \cdot \left(i\omega C_{coating}\right)}{\left(i\omega C_{coating}\right) \cdot \left[1 + R_{DE} \cdot T_{DE} \cdot (i\omega)^{\phi}\right]} \quad (8)$$

A physical reasoning was also established for the use of the Zarc-Cole element. This justification was based heavily on geometry. It has been known that distributed elements , specifically the constant phase element, model the electrical responses for rough surfaced systems [7]. In the system under study, the grit blast cleaning of the steel surface creates a rough non-parallel surface. This, compounded with a coating, significantly slows the response signal from the steel surface. Therefore, the retarded response would be best modeled by the distributive element.

3.2.2 Capacitance vs. Delamination Trends

The purpose of this study was to determine if electrochemical impedance spectroscopy could be used as an effective tool to predict delamination for long times via capacitance measurements made during the early stages of coating evaluation The analysis of this study focused on samples tested up till Day 6 because capacitance measurements began to show erratic behavior beginning around Day 8 and continued throughout the duration of the study. This is clearly seen in Figure 17 which shows the capacitance data for samples tested for 16 and 20 days. Capacitance values either plateau or decrease at or around this point. It is difficult to attribute this phenomena to any one particular cause but one hypothesis is presented.

Occlusion of the surface by hydrogen gas which is generated by the reduction of water could explain this irregular behavior of the capacitance. Trapped hydrogen gas bubbles can mask of reactive areas to the applied signal; as a result the true delaminated area is undermeasured by the capacitance magnitude.

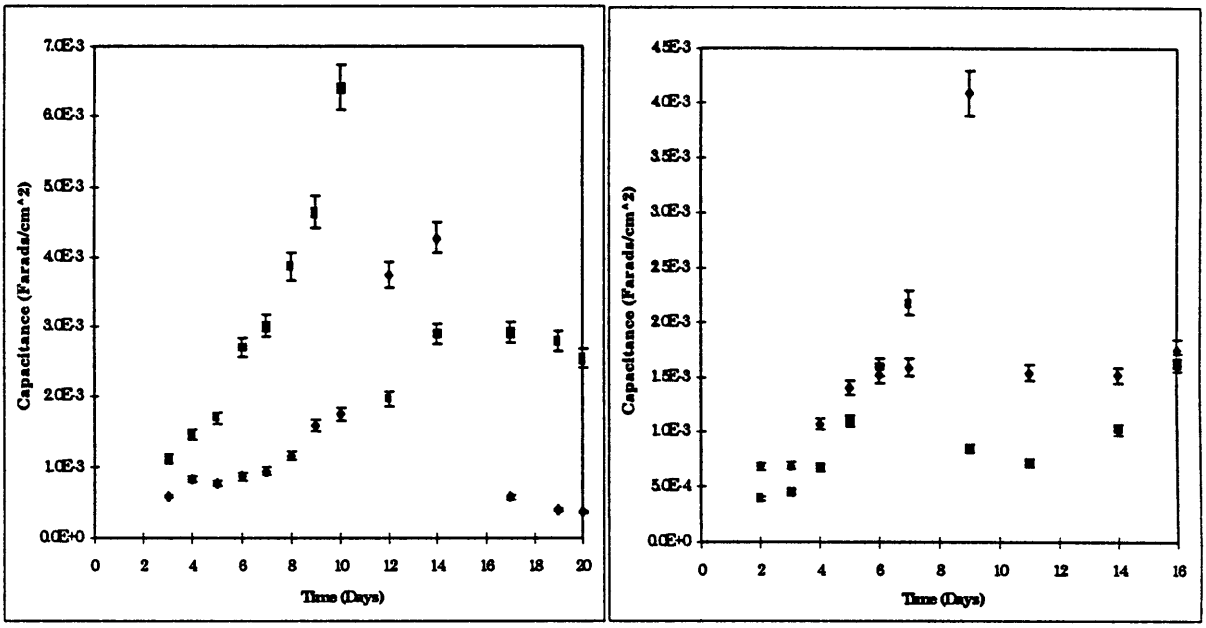

a) b)

Figure 17 Samples run for a)16 days and b) 20 days; samples are fit with error bars of 5% associated with the error in measuring the impedance of the samples. There is an increase in capacitance of the samples up to Day 8 or Day 10 followed by a plateauing or drop in capacitance thereafter. This phenomena could be attributed to hydrogen entrapment which would mask the reactive areas.

Figures 18,19, and 20 show the capacitance vs. average calculated delamination for samples tested for 2, 4, and 6 days respectively. In most cases, it appears that the factor which relates delamination area to capacitance is between $2 * 10^{-5}$ and $5 * 10^{-5}$

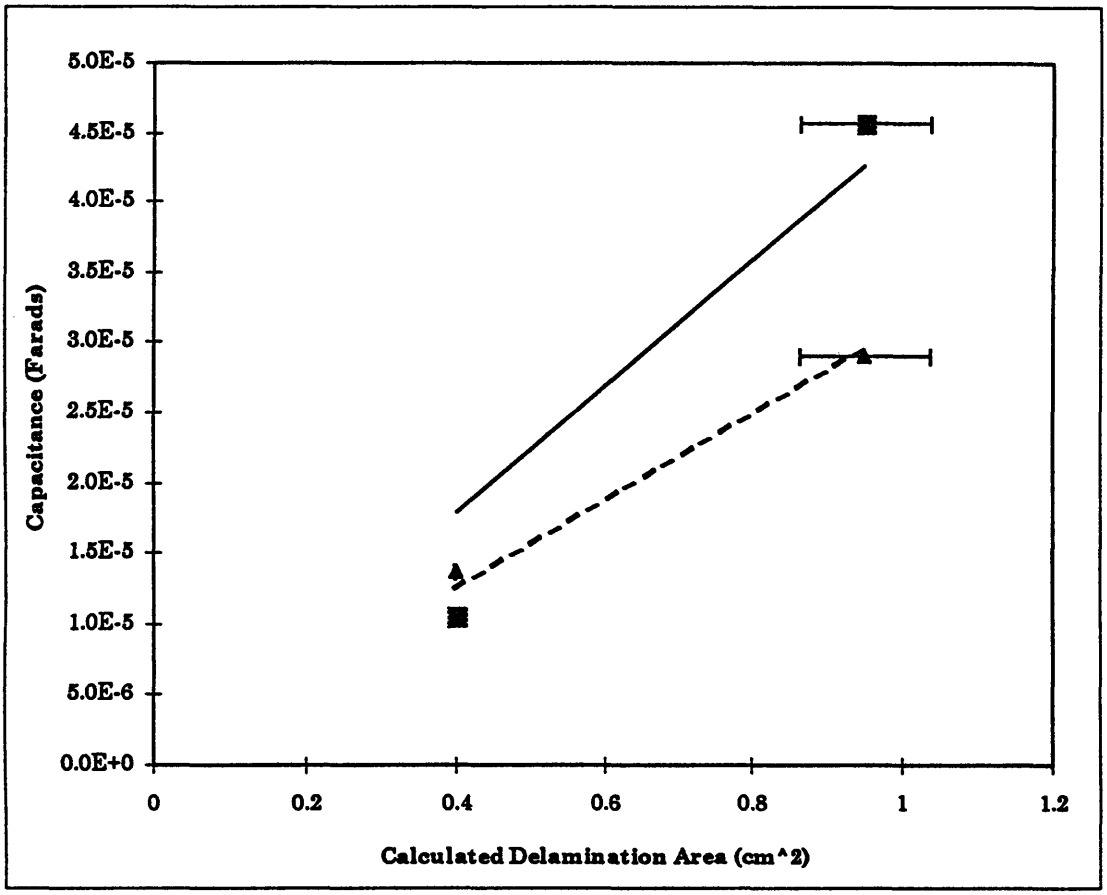

Figure 18. Day 2 capacitance vs. average calculated delamination trends from two individual samples. Error bars are drawn in to show the variability in delamination during testing. Linear trendlines are fit to the data and the constants relating delamination area to capacitance from these trendlines are $4*10^{-5}$ Farads/cm^2 for the and $3*10^{-5}$ Farads/cm^2 for the ■ and ▲ data points respectively.

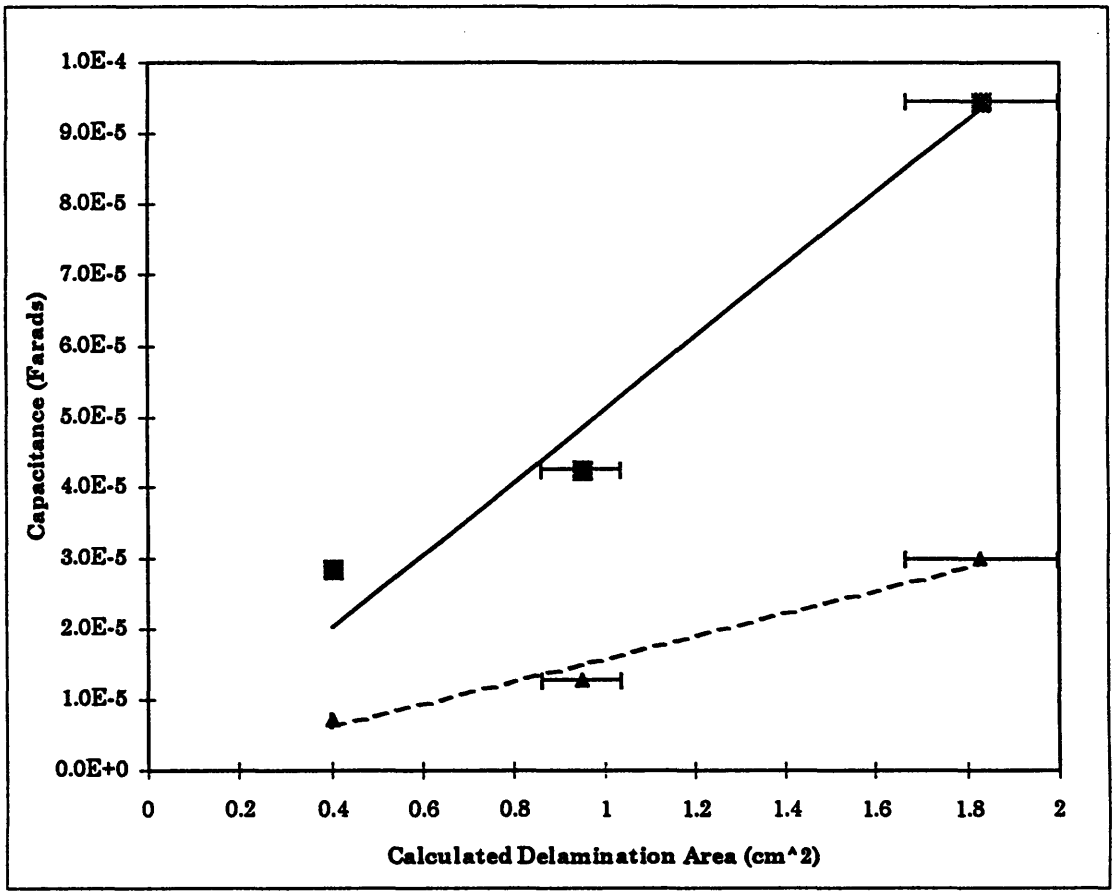

Figure 19. Day 4 capacitance vs. average calculated delamination trends from two individual samples. Error bars are drawn in to show the variability in delamination during testing. Linear trendlines are fit to the data and the constants relating delamination area to capacitance from these trendlines are $5*10^{-5}$ Farads/cm^2 for the and $3*10^{-5}$ Farads/cm^2 for the ■ and ▲ data points respectively.

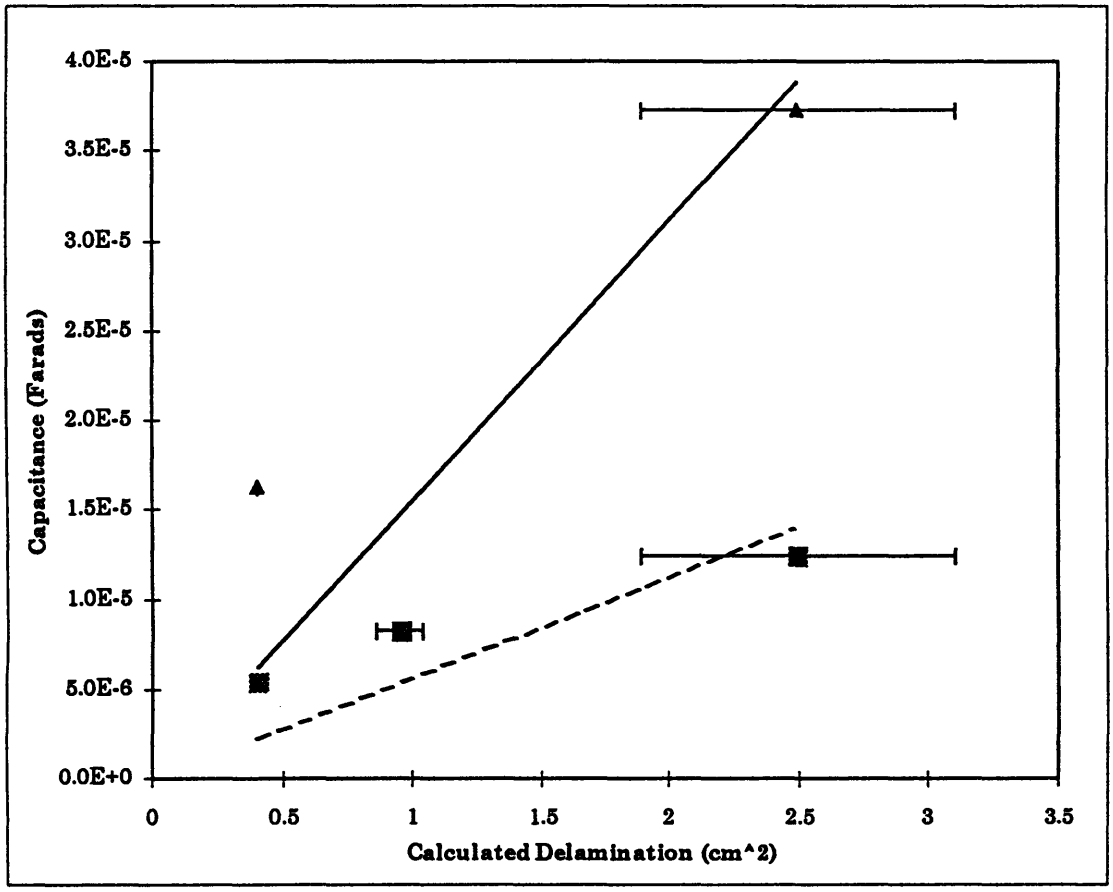

Figure 20. Day 6 capacitance vs. average calculated delamination trends from two individual samples. Error bars are drawn in to show the variability in delamination during testing. Linear trendlines are fit to the data and the constants relating delamination area to capacitance from these trendlines are $6*10^{-6}$ Farads/cm^2 for the and $2*10^{-5}$ Farads/cm^2 for the ■ and ▲ data points respectively.

Farads/cm^2. The variability in the observed delamination indicates that this factor could be relatively constant between different samples.

The poor fitting of trendlines in both Day 2 and Day 6 samples call for careful interpretation of the data. In the Day 2 measurements (Figure 18), the poor fit of the trendline to the square data points is difficult to explain. Care must also be used when analyzing the trends in Figure 20 because of the large variation in the calculated delamination area. The sample with the triangle data points shows a proportionality constant an order of magnitude lower than that observed for all other samples. Early occlusion of the samples could explain this since the capacitance underestimates the delamination.

The previous figures indicate that when variability in delamination area is considered, the factor $\kappa\varepsilon_0/d$ which relates capacitance and delamination area is relatively constant. Therefore, there appears to be a correlation between capacitance and delamination.

Based on this correlation, the prediction abilities of this experimental technique were analyzed using the data from Day 4 specimens because those samples had the best fit trendlines. Upon generation of capacitance vs. time plots fit with linear regression for the two samples in Figure 19, capacitances were estimated using equations 9 and 10 for times greater than 4 days. These estimated capacitances were then inserted into equations 11 and 12, which describe the behavior of the capacitance vs. average calculated delamination plots, to arrive at predicted delamination areas. These values were then compared to the

Table 3 Linear fit equations used to estimate capacitance values (equations 9 & 10) and predict delamination (equations 11 & 12) from Day 4 specimens.

Sample	Capacitance vs. Time	Capacitance vs. Delamination
■	Capacitance=$2*10^{-5}$*(Time) (9)	Capacitance=$5*10^{-5}$*(Delamination) (11)
▲	Capacitance=$7*10^{-6}$*(Time) (10)	Capacitance=$2*10^{-5}$*(Delamination) (12)

Table 4. Predicted vs. observed delamination values. Percent error is given for both the observed delamination and the predicted delamination.

Time (Day)	Predicted Delamination Sample 1 (▲) (cm^2)	Predicted Delamination Sample 2 (■) (cm^2)	Observed Delamination (cm^2) (Error %)	Error Sample 1 (%)	Error Sample 2 (%)
6	2.1	2.4	2.5 (84)	15	3
8	2.8	3.2	3.1 (38)	9	4
10	3.5	4.0	5.3 (100)	33	24
12	4.2	4.8	3.6 (10)	16	33
14	4.9	5.6	5.1 (25)	4	9
16	5.6	6.4	7.9 (25)	30	19
18	6.3	7.2	9.4 (17)	33	23
20	7.0	8.0	10.9 (81)	36	26

average observed delamination area seen over the 20 day testing period. Table 3 shows the fit equations which were obtained from the Day 4 samples. Table 4 shows the observed and predicted delaminations; error is described as the difference between the two measurements as a percentage of the observed delamination.

The results from the predicted delamination areas shows close correlation to the observed delamination areas up to approximately Day 14 even though a large error is seen with sample at Day 10. Predicted delamination areas between Day 16 and Day18 show errors values between 20 and 35%; if the variation in delamination areas are taken into consideration, these error values would fall. It is difficult to determine how predicted values compare with observed values in Day 20 specimens because of the tremendous variability in delamination at this time. However, when compared to the existing cathodic disbondment test method, the repeatability would be better when using this test method.

3.2.3 EIS as a Delamination Predicting Tool

This EIS prediction tool can be utilized in two manners. First, as displayed in Table 4, delamination areas can be predicted based only on numerical analysis. Second, by using the equations in Table 3 to predict delamination from Day 1 to Day 4 and then fitting these values with a trendline, delamination areas for times up to Day 14 and even Day 16 can be obtained as seen in Figure 21.

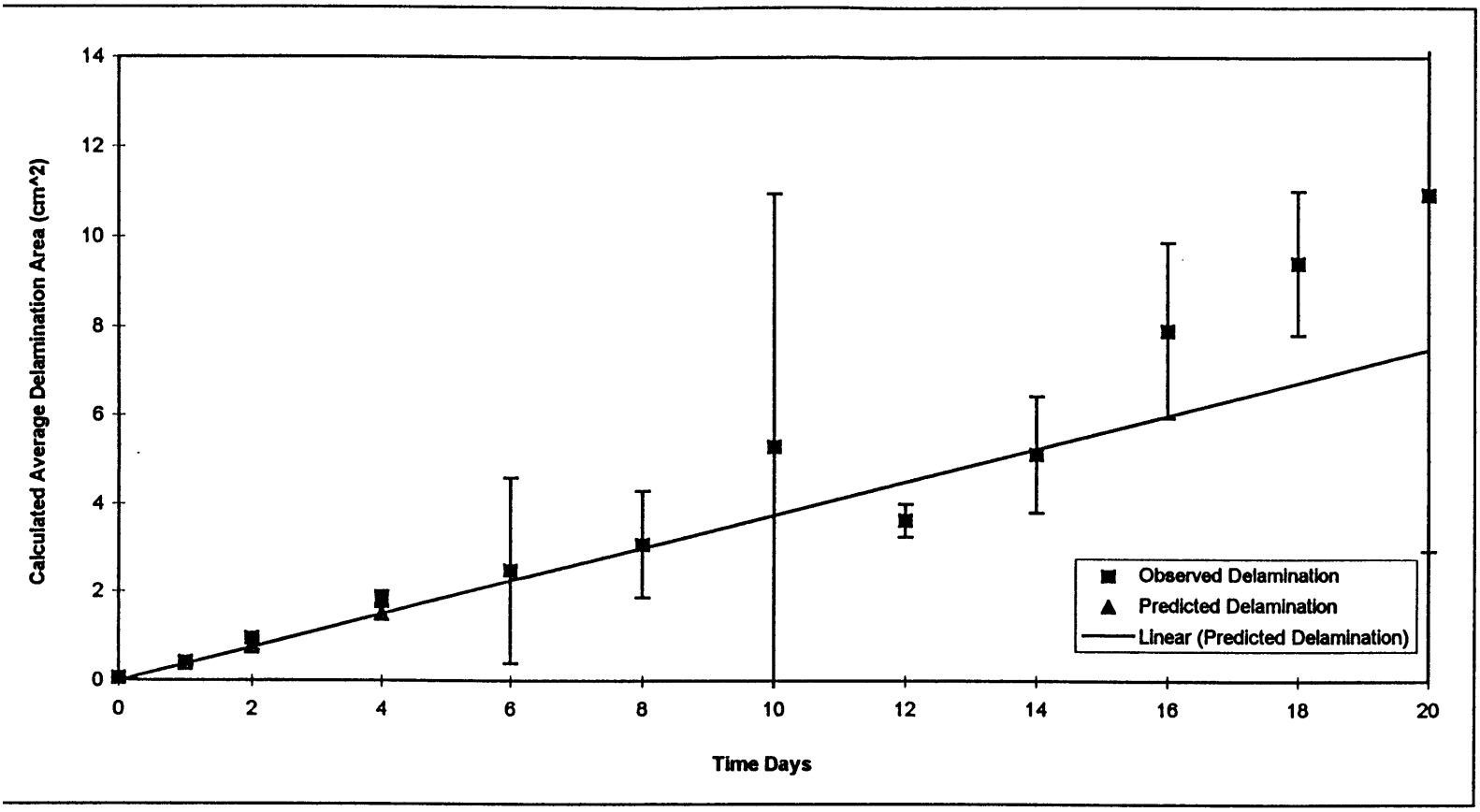

21. Plot of observed delamination over the twenty day test. Predicted delamination areas from Day 0 to Day 4 are overlaid. Linear regression was performed on the predicted areas. The fit trendlines indicates that delamination area can be predicted up to Day 14 or even Day 16 based on early delamination estimations.

3.2.4 Summary

From this analysis, it has been shown that EIS can be an appropriate method for measuring delamination with capacitance in this setup. Using EIS offers the advantage of delamination prediction by measuring a few samples (about 2 specimens *in situ*) rather than the 2 samples per day required (total of 6 to 10 specimens) for the conventional ASTM Standard G8 cathodic disbondment test. In addition, this EIS techniques allow for observation of delamination without disruption of the electrochemical cell. These two important advantages make the EIS technique a powerful tool in coating evaluation.

3.3 Temperature and pH effects

3.3.1 Introduction

The effects of temperature and pH on epoxy coated steel plates kept under a -3V vs. SCE polarization in 3 wt% NaCl solution were studied to try and further the delamination prediction capabilities in coating evaluation. Such relationships would allow prediction of delamination at various temperatures and pHs by simply obtaining delamination measurements (either through actual testing or predictive delamination from the EIS techniques) at either one temperature or one pH. This could prove to save valuable time during the coating evaluation process.

3.3.2 Temperature effects on Delamination

Cathodic disbondment tests may be performed at two or three temperatures to accelerate the effects. However, in order to observe delamination at these different temperatures, 2 to 3 sets of samples must be tested. If delamination can be predicted based from simple relationships, valuable time can be saved. Then, using this predictive tool, coating delamination can be estimated for various climates.

It is hypothesized that delamination should exhibit an Arhennius type behavior because it is most probably dependent upon the chemical reaction of water and oxygen

being reduced and creating hydroxide groups which attack the polymer/metal interface. As with other chemical reaction mechanisms, the one in this study should be dependent upon the temperature and a characteristic activation energy. The radius of delamination was followed because it is hypothesized that delamination is an interface phenomena.

This Arhennius type of behavior is further explained through equation 13,

$$R = R_0 \cdot \exp\left(\frac{-E_{activation}}{RT}\right) \tag{13}$$

where R is the delamination rate (millimeter radius (mmr) disbondment/day), R_0 is the constant of the equation (mmr/day), $E_{activation}$ is the activation energy (Joules/mole) , R is the molar gas constant (8.314 Joules/mole*Kelvin), and T is the temperature (Kelvin).

Figure 22 shows the results from the fitting of delamination points from two separate experiments run for 6 days and 10 days. Specimens were tested at room temperature (22 ^{0}C), 65 ^{0}C, and 80 ^{0}C for both test durations. In the analysis, the data from Day 6 and Day 10 were consolidated into one plot by converting to a delamination rate (millimeter radius/day (mmr/day). An activation energy ($E_{activation}$) of 330 Joules/mole (~80 cal/mole) as calculated from the plot in Figure 22.

In analyzing the data from Figure 22, it appears that delamination rate displays a linear trend when plotted against the inverse of temperature indicating that this rate fits the Arhennius type behavior nicely. However, the calculated activation energy is 2 to 3

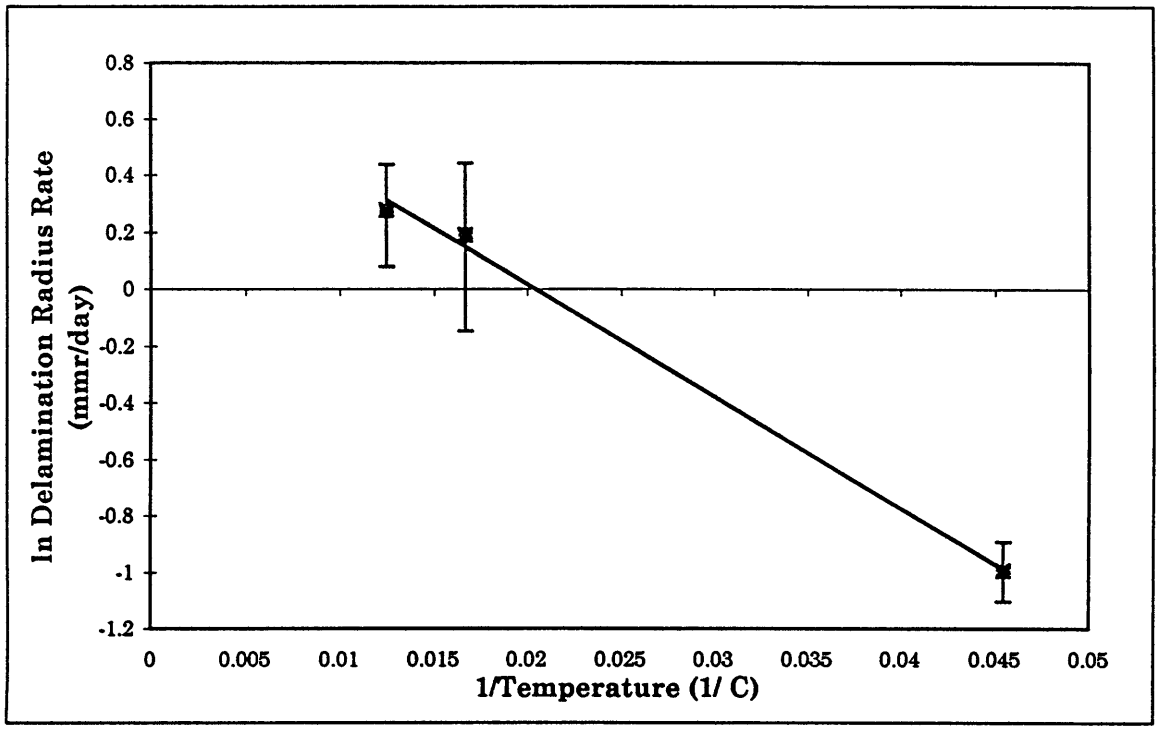

Figure 22 Inverse temperature vs. ln delamination rate plot for epoxy-coated steel samples tested at three temperatures (22 ^{0}C, 65 ^{0}C, 80 ^{0}C correspond to .045, .015, and .0125 on inverse temperature axis). Error bars are included to show variation in delamination rate for individual test temperatures. Regression through these points indicates a good fitting of the data. $E_{activation}$ was calculated to be around 330 Joules/mole.

orders of magnitude less than those observed with chemical reactions. In addition, the doubling of the delamination rate every 4.4^{0}C as observed by Nehete produces a activation energy around 118 KJoules/mole if this reaction behaves in an Arhennius fashion [1]. The activation energy calculated from this study most probably indicates that the delamination rate is governed by more then the one mechanism considered in this study. This could be a complex chemical mechanism or a physical mechanism. In order to determine if this is the case, a more detailed study must be undertaken with more information about the delamination rate from the intermediate temperatures.

3.3.3 pH effects on Delamination

pH effects on coating delamination were also studied even though present cathodic disbondment test methods do not require such an investigation. A pH study is significant because the environment around coated pipes varies from region to region. Such changes can have drastic effects on delamination. Therefore, this study was taken on to determine if a scaling factor could be obtained for prediction of delamination over a wide range of pHs. If successful, this relationship could be utilized to predict coating delamination in the different regions based on laboratory testing such that economical and ecological disasters could be averted.

It has been shown that pH has a effect on delamination; in basic environments delamination is higher than in neutral environments while in acidic environments, delamination is decreased [27]. In addition, it has been observed that with defect sites, the local pH increases and finally stabilizes. The sodium chloride electrolyte which began with a pH between 7 and 8 increase and stabilized to pH values between 9 and 10. The sample electrolyte which started at a pH of 1 increased and stabilized to values between 3 and 4 by the end of the testing. This can be explained by the reduction of water and oxygen around the defect site which creates hydroxide groups. The hydrogen gas produced harmlessly escapes.

In this study, delamination was studied in both pH adjusted (pH ~ 1) and ambient pH electrolytes (pH ~ 8) at 65 ^{0}C at -3V vs. SCE in 3 wt% NaCl solutions. However, the individual potentiostat cards in the multiplexer could not sustain the required -3V vs SCE

polarization on the samples which were at the pH of 1. The potential sustained by the sample was around -2.5V vs. SCE. This is attributed to the excess H^+ concentration in the electrolyte which would pass large amounts of current and as a result could not sustain the required prescribed potential. Tests were performed even though this was the case. Figure 23 shows the results from the pH study.

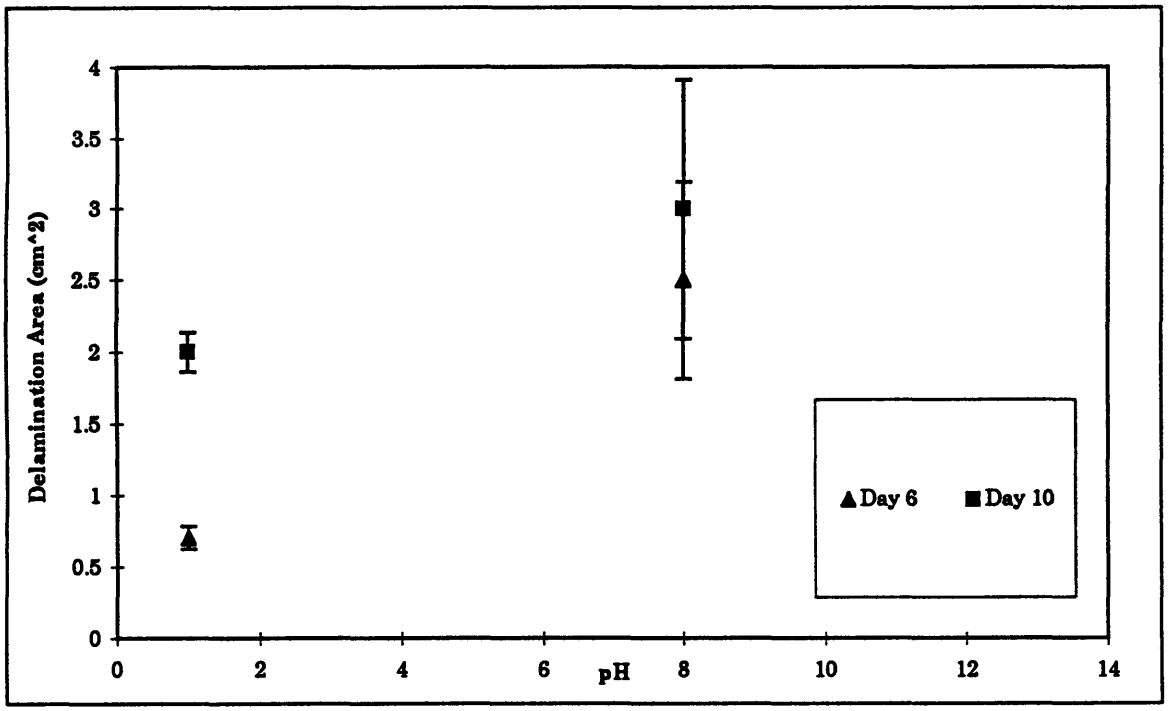

Figure 23. Results from the pH effects on delamination of epoxy coated steel samples run under cathodic polarization. The results indicate that delamination is limited at the lower pH values probably due to decreased hydroxide production.

Both samples show that there is a decrease in delamination at the lower tested pH. This decrease in delamination area can be attributed to limited generation of hydroxide groups at this low pH. These groups are primarily responsible for coating delamination

through attack of the polymer, the oxides on the metal, and through attack of the metal/polymer interface. [7].

There is a no doubt that delamination decreases in acidic test conditions; the samples tested show a 2-2.5X decrease in delamination from the pH 8 to pH 1. However, it is not possible to predict delamination at the intermediate pHs because the electrochemistry increases the pH of the local environment; the samples become more basic with time through the production of the hydroxide groups. This change in pH complicates prediction capabilities. However, this study has shown that delamination is reproducible at pH 1 and 8.

In order for this test method to be reliable in predicting delamination at various pH values, extrapolations between the points shown in Figure 23 must be made. Then tests at the intermediate pHs must be performed. If the observed delaminations occur at or around the extrapolated lines, then this test method could be used as a prediction tool for various pHs.

3.3.4 Summary

Both temperature and pH effects on delamination prediction have been studied. Preliminary conclusions indicate that predictions probably can not be made unless other complicated mechanisms are considered. However, further work in these two areas could lead to a valuable new tool for coating delamination predictions at various temperatures and pHs through EIS techniques which would save time during the coating evaluation process.

4 Conclusions and Future Work

4.1 Conclusions

The goal of this study was to determine if electrochemical impedance spectroscopy (EIS) could be used as a tool to predict delamination through non-intrusive methods via capacitance measurements made during the early stages of coating evaluation. The success of such a predictive technique is dependent upon a consistent relationship between measured capacitance and average calculated delamination area. From such a correlation, predictions in delamination area for extended times could be made through estimations of capacitance values.

This study reveals that delamination is tied directly to the measurable quantity of capacitance which can be obtained from impedance scans. Therefore, EIS is an appropriate method to predict delamination if the following factors are considered: a consistent increase in delamination produces a corresponding increase in measured capacitance, capacitance and time increase in a linear fashion, and that capacitance measurements at times later than Day 8 do not accurately represent delamination due to occlusion of the surface. Using this technique, delamination can be numerically estimated for times up to Day 14 with good accuracy; predictions for Days 16-20 are off by approximately 20- 35%. These error values diminish when the variations in observed delaminations are considered and compared with the predicted delamination values.

Accurate predictions of delamination can also be obtained till day 14 by fitting trendlines to predicted delamination values from the first 4 days.

Temperature and pH delamination predictions were also studied. Initial observation of the temperature effects indicate that delamination rate behaves in and Arhennius type fashion. However, the calculated activation energy of 330 Joules/mole is a few orders of magnitude lower then those observed from other reactions; this indicates that either a more complicated behavior than the one considered in this study occurs or that the delamination rate behaves in some other manner. The results from the pH study indicate that there is a 2-2.5X decrease in delamination at the lower tested pH. However, because the local pH of the system constantly increases from the original pH, it is not possible to predict delamination for a range of pHs.

4.2 Suggestion for Future Study

1. Although this analysis protocol should apply for any coating, this should be confirmed with other coatings using this exact test method. If similar results are found, then EIS can be used as an effective tool to predict delamination without going through the time consuming process of actual testing.

2. The effects of temperature needs to be further analyzed. The activation energy which was calculated for this system appears to be a few orders of magnitude too small for it to considered a chemical reaction. Therefore, to determine if delamination rate behaves in a more complex Arhennius fashion or some other behavior, delamination rates at intermediate temperatures needs to be charted.

3. A study should be undertaken to determine if the delamination follows trendlines fit to the data in the pH study. If a close fit is obtained, then the increase in pH during testing should not play as significant a role in predicting delamination. As a result, coating delamination can be estimated for a whole spectrum of climates through laboratory testing.

5 Bibliography

1. Nehete, M.H. "Pipeline Coatings" *PaintIndia* p. 53-64. May 1989.
2. Uhlig, Herbert H., Revie, R. Winston. Corrosion and Corrosion Control: An Introduction to Corrosion Science and Engineering. Chapters 6, 12, 15, & 18. John Wiley & Sons, New York, 1985.
3. Fink, K., Payer, J.H., Savinell, R. "Mitigation of Corrosion by Modification of the Environment Beneath Disbonded Coatings on Pipelines." *Corrosion 93-The NACE Annual Conference and Corrosion Show.*
4. Jones, Denny A. Principles and Prevention of Corrosion. Chapter 2. McMillian Publishing Co. New York, 1992.
5. Ragone, David V. Thermodynamics of Materials. Chapter 6. John Wiley and Sons. New York, 1995.
6. Pourbaix, Marcel (author), Green, J.A.S., (translator), Staehle, Roger W. Lectures of Electrochemical Corrosion. Chapter 4. Plenum Press, New York. 1973.
7. 3M Company Austin, TX - Internal Correspondence
8. ASTM: G8 - 90, "Standard Test Methods for Cathodic Disbonding of Pipeline Coatings." ASTM, Philadelphia (1990).
9. Bard, A.J., and Faulkner, L.R. Electrochemical Methods : Fundamentals and Applications. Cover Flap. John Wiley and Sons. New York, 1980.
10. British Gas - Gas Business Engineering - Technical Specifications for the External Protection of Steel Line Pipe and Fittings Using Fusion Bonded Powder and Associated Coating Systems. Part 1 - Requirements for Coating Materials and Methods of Test. January 1993.
11. National Standards of Canada - External Fusion Bond Epoxy Coating for Steel (CAN/CSA-z245.20-M92), External Polyethylene Coating for Pipe (CAN/CSA-Z245.21.M92). March 1992.
12. Personal Communication with Dr. Alan Kehr, 3M Co. Austin, TX.
13. Nenov, Krassimir P. "Impedance Spectroscopy of Water Uptake and Long Term Degradation of Immersed Polyimide Coatings." Ph.D. Dissertation DMSE, MIT, Cambridge, MA (1994).
14. Titz, J., Wagner, G.H., Spahn, H., Ebert, M., Juttner, K., Lorenz, W.J. *Corrosion*, 46 (3) 221-229, 1990.
15. Quintela, J.P., De Oliveira, R.C.A., Margarit, I.C.P., Mattos, O.R. *Materials Science Forum.* **192-194.** 308-316. 1995.
16. van Westing, E.P.M., Ferrari, G. M., de Wit, J.H.W. *Corrosion Science*. **36**(6) 979-994, 1994.
17. Personal Communication with Dr. Maureen Fahey, 3M Company Austin, TX.
18. Schueller, Gayle. "The Nondestructive Evaluation of Adhesive Disbondment in Al/Polymer Laminates by Electrochemical Impedance Spectroscopy." Ph.D. Dissertation. School of Engineering and Applied Science, UVA Charlottesville, VA (1992).

19. Miskovic-Stankovic, V.B., Deflorian, F., Bonora, P.L., Fedrizzi, L. *Journal of the Serbian Chemical Society.* **61**(7) 591-600, 1996.
20. Halliday, D., Resnick, R., Krane, K.S. Physics, Vol. 2 John Wiley & Sons, Inc. New York. 1992.
21. Zhang, S.H., Lyon, S.B. "Problems in A.C. Impedance Measurements of High Resistance System in Thin-Film Electrolytes." Electronics Division Colloquium on Electrochemical Measurements Digest # 1994/07. The IEE London, 1994.
22. van der Weijde, D.H., van Westing, E.P.M., de Wit, J.H.W. *Corrosion Science* **36** (4) 643-652 (1994).
23. Deflorian, F., Fedrizzi, L., Bonora, P.L. *Electrochimica Acta* **38** (12) 1609-1613, 1993.
24. Katayama, H., Nishikata, A., Tsuru, T. *Electrochimica Acta*, **41** (7) 1093-1097, 1996.
25. Katayama, H., Nishikata, A., Tsuru, T. *Zairyo-to-Kankyo* **45** (5) 292-297. 1996. (Japanese)
26. Data acquisition through ZPlot and data analysis through Zview from Scribner Associates, Inc.
27. McHattie, J.S., Perez, I.L., & Kehr, J.A. *Cement & Concrete Composites.* **18** 93 103. 1996.

6 Biographical Note

The author was born in Madras, India and emigrated to the United States early in his childhood. After exposure to the concepts of materials engineering from relatives in the field, he became very interested in engineering, especially materials science and engineering. At this point, his goal was to attend the Massachusetts Institute of Technology. In the fall of 1992, this opportunity was made available to him. There, he majored in materials science and engineering and enjoyed his time as a student-athlete in the Department of Materials Science and Engineering and with the Heavyweight Crew Program. After graduation with an SB in 1996, he pursued a graduate degree in the area of materials science and engineering through a special program MIT offered. Spending one semester in Austin TX with the 3M Company, he completed the research for his masters degree. The following semester, he returned to MIT where he completed his masters degree in June 1997. Upon completion of his masters degree, he pursued an opportunity at the 3M Company in Austin, TX in the Telecom Systems Division.